

See discussions, stats, and author profiles for this publication at:
<https://www.researchgate.net/publication/260201264>

Evaluation of Various Surface Wind Products with OceanSITES Buoy Measurements

Article *in* Weather and Forecasting · December 2013

Impact Factor: 1.79 · DOI: 10.1175/WAF-D-12-00086.1

CITATIONS

3

READS

44

7 authors, including:



[Ge Peng](#)

North Carolina State University

32 PUBLICATIONS 289 CITATIONS

SEE PROFILE



[Huai-Min Zhang](#)

National Oceanic and Atmospheric Admi...

35 PUBLICATIONS 799 CITATIONS

SEE PROFILE



[Jean Bidlot](#)

European Center For Medium Range We...

83 PUBLICATIONS 9,637 CITATIONS

SEE PROFILE



[Scott Edward Stevens](#)

North Carolina State University

3 PUBLICATIONS 4 CITATIONS

SEE PROFILE

Evaluation of Various Surface Wind Products with OceanSITES Buoy Measurements

GE PENG,* HUAI-MIN ZHANG,[†] HELMUT P. FRANK,[#] JEAN-RAYMOND BIDLOT,[@]
MASAKAZU HIGAKI,[&] SCOTT STEVENS,* AND WILLIAM R. HANKINS**

* CICS-NC, North Carolina State University, and NOAA/National Climatic Data Center, Asheville, North Carolina

[†] NOAA/National Climatic Data Center, Asheville, North Carolina

[#] Deutscher Wetterdienst, Offenbach, Germany

[@] ECMWF, Reading, United Kingdom

[&] Japan Meteorological Agency, Tokyo, Japan

** ERT, Inc., and NOAA/National Climatic Data Center, Asheville, North Carolina

(Manuscript received 10 September 2012, in final form 5 April 2013)

ABSTRACT

To facilitate evaluation and monitoring of numerical weather prediction model forecasts and satellite-based products against high-quality in situ observations, a data repository for collocated model forecasts, a satellite product, and in situ observations has been created under the support of various World Climate Research Program (WCRP) working groups. Daily measurements from 11 OceanSITES buoys are used as the reference dataset to evaluate five ocean surface wind products (three short-range forecasts, one reanalysis, and one satellite based) over a 1-yr intensive analysis period, using the WCRP community weather prediction model evaluation metrics. All five wind products correlate well with the buoy winds with correlations above 0.76 for all 11 buoy stations except the meridional wind at four stations, where the satellite and model performances are weakest in estimating the meridional wind (or wind direction). The reanalysis has higher cross-correlation coefficients (above 0.83) and smaller root-mean-square (RMS) errors than others. The satellite wind shows larger variability than that observed by buoys; contrarily, the models underestimate the variability. For the zonal and meridional winds, although the magnitude of biases averaged over all the stations are mostly $<0.12 \text{ m s}^{-1}$ for each product, the magnitude of biases at individual stations can be $>1.2 \text{ m s}^{-1}$, confirming the need for regional/site analysis when characterizing any wind product. On wind direction, systematic negative (positive) biases are found in the central (east central) Pacific Ocean. Wind speed and direction errors could induce erroneous ocean currents and states from ocean models driven by these products. The deficiencies revealed here are useful for product and model improvement.

1. Introduction

Accurate global high-resolution surface winds and related momentum fluxes (surface stresses) are critical for improving numerical weather prediction (NWP) and climate model forecast skills, and are essential to ocean modeling and marine forecasting (Josse et al. 1999; Curry et al. 2004; Large et al. 1991; Bourassa et al. 2010). Earlier NWP forecast or analysis winds fall short in representing the temporal and spatial variability of synoptic-scale systems. For example, the coarse spatial resolution in the National Centers for Environmental Prediction–National Center for Atmospheric Research

(NCEP–NCAR) reanalysis (with a horizontal resolution of $2.5^\circ \times 2.5^\circ$) could offset the center of a synoptic-scale cyclonic eddy that occurred in October–November 1996 by nearly 3° compared to satellite-based winds derived from National Aeronautics and Space Administration Scatterometer (NSCAT) along-swath measurements (Peng 2004). On the regional scale, the surface winds from the National Meteorological Center (NMC, now known as NCEP) 80-km operational regional Eta Model were insufficient to model the local spatial variability of surface winds in south Florida when compared to in situ observations from April 1994 to April 1995 (Peng et al. 1999). The tropical Pacific surface wind analyses from the low-resolution models of NMC, the Met Office, and the European Centre for Medium-Range Weather Forecasts (ECMWF) compared poorly with the Tropical Atmosphere Ocean (TAO) buoy winds for the period of

Corresponding author address: Dr. Ge Peng, CICS-NC, NOAA/NCDC/RSAD, 151 Patton Ave., Asheville, NC 28801.
E-mail: ge.peng@noaa.gov

February–July 1987, with a bias as large as 3.1 m s^{-1} (Reynolds et al. 1989). At that time, the TAO buoy data were not assimilated in any of these three analyses but have been since and have also been proven to be valuable in validating model and remote sensing products; a comprehensive review of the Tropical Ocean Global Atmosphere (TOGA) observing system and its application can be found in McPhaden et al. (1998).

Satellite measurements have been shown to be capable of resolving small-scale features (Cornillon and Park 2001; Kelly et al. 2001; Chelton et al. 2004; Tang et al. 2004). Assimilating the Quick Scatterometer (QuikSCAT) observations, which provide estimates of both wind speed and direction over the oceans, has shown improvements in the accuracies of 10-m wind analyses from the operational ECMWF and NCEP NWP models (Chelton and Freilich 2005). In that case, buoy data had already been assimilated into the models.

Many international modeling centers are assimilating both in situ and remotely sensed measurements and are now producing global high-resolution surface winds. The World Climate Research Program (WCRP) Working Groups on Numerical Experimentation and on the Surface Fluxes (WGNE and WGSF), Observation and Assimilation Panel (WOAP), and the Ocean Observation Panel for Climate (OOPC) have initiated the Surface Fluxes Analysis (SURFA) project to evaluate the performance of global NWP forecast winds. This effort was recently further endorsed by the Action Plan for WCRP Research Activities on Surface Fluxes (WCRP 2012). A collocated in situ and NWP model data repository center has been established at the National Climatic Data Center (NCDC; www.ncdc.noaa.gov/thredds/surfa.html), which is also one of the data centers for the National Oceanic and Atmospheric Administration's (NOAA's) satellite and other climate data, to facilitate the evaluation and monitoring effort of weather and climate model forecast skills and satellite-based products against high-quality in situ observations. A predefined horizontal grid for all NWP models has been agreed upon, which minimizes the effort and potential errors of collocating data from different data grids at the user end.

With the recent NCEP release of its latest Climate Forecast System Reanalysis (CFSR; Saha et al. 2010), it is of interest to various user communities to see how well its wind product compares with observations and other wind products.

A satellite-based blended ocean surface wind dataset has been produced routinely at NCDC as a research product (Zhang et al. 2006). As the NCDC blended sea wind product becomes more accepted in the user community for research, modeling, and monitoring-related

projects, there has been increasing demand to provide some qualitative evaluation of the product in various regions, as well as ways to improve it.

As a first step in evaluating the performance of the global NWP forecast winds, Peng et al. (2011) have compared short-range forecast winds from three global high-resolution NWP models, together with the NCDC blended ocean surface winds and the CFSR surface winds, against high-quality in situ observations at three locations in the equatorial Pacific Ocean. They have uncovered a negative (positive) directional bias in the central (east central) Pacific Ocean. Here, we expand that work to 8 more stations, for a total of 11 station locations in the Indian, Pacific, and Atlantic Oceans.

In situ measurements are valuable when validating satellite-derived products (Freilich and Dunbar 1999; Ebuchi et al. 2002; Freilich and Vanhoff 2006; Abdalla et al. 2011). Most previous satellite, model, and in situ wind comparisons have been focused on absolute speed only (Mears et al. 2001). This is because most derived variables of remotely sensed measurements, such as those derived from microwave radiometers, only provide wind speeds and do not provide directional information. The availability of satellite wind vectors, such as those derived from scatterometer measurements, allows for comparisons that do include wind direction. They have proven to be useful in identifying directional errors in buoy measurements (Dickinson et al. 2001) and models (Brown et al. 2005) and, therefore, have led to improvements in buoy measurements (Dickinson et al. 2001). The purpose of SURFA is to reveal temporal and spatial biases in the NWP forecast winds to improve NWP surface flux products including the vertical momentum flux (surface stress). Since zonal and meridional (u , v) components of the winds, rather than wind speeds, are NWP forecast variables and inputs for computing surface wind stresses and the stress curl, the focus will be on the biases in u and v of these wind products against point observations. However, wind speed and directional biases will also be examined for completeness.

2. Data

The wind data and products used in this study consist of four categories: 1) observed in situ winds, 2) satellite-based blended and gridded winds, 3) NWP short-range forecast winds, and 4) reanalysis winds.

a. In situ winds from OceanSITES

The high-quality in situ reference observations are wind measurements from OceanSITES, a global network of open-ocean sustained time series sites as an integral

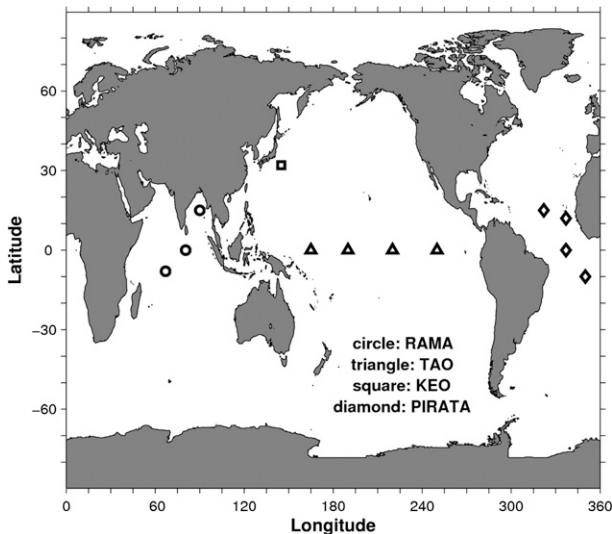


FIG. 1. Location of the RAMA (circles), KEO (square), TAO (triangles), and PIRATA (diamonds) buoys in the OceanSITES network.

part of the Global Ocean Observation System (<http://www.oceansites.org>). There are 12 buoy stations in the OceanSITES network that provide surface wind measurements (Fig. 1), consisting of three Research Moored Array for African–Asian–Australian Monsoon Analysis and Prediction (RAMA) buoys in the Indian Ocean (McPhaden et al. 2009), four Tropical Atmosphere Ocean (TAO) moorings (McPhaden et al. 1998), one Kuroshio Extension Observatory (KEO) buoy (Cronin et al. 2008; Donohue et al. 2008), and four Prediction and Research Moored Array in the Tropical Atlantic (PIRATA) buoys (Bourlès et al. 2008).

The analysis presented here is with wind data for the year 2009, the SURFA intensive analysis period that contained the most complete 1-yr wind records for both model and in situ datasets from the participating institutions when this analysis began. The data from

the eastern equatorial Pacific Ocean (0° , 110°W) station are not included in the analysis as less than 2 months of buoy data are available. One midlatitude buoy station (the KEO buoy located at 32.4°N , 144.6°E in the Pacific Ocean) is included, together with 10 tropical OceanSITES stations (three RAMA buoys in the tropical Indian Ocean, three TAO moorings in the equatorial Pacific Ocean, and four PIRATA buoys in the tropical Atlantic Ocean). (See Table 1 for station IDs and attributes; the station IDs will be used in the following text and figures except where the geolocation is emphasized; then, the latitude and longitude values will be used.) The winds from these 11 OceanSITES stations will be referred to as the OS winds hereafter. These winds are measured at a height of 4 m, with an accuracy of about 0.3 m s^{-1} for wind speed and about 1.0° for wind direction (Freitag et al. 2001). For comparison with other wind products, these 4-m buoy winds are adjusted to 10-m height, as detailed in section 3.

b. Remotely sensed blended sea surface winds

Sea surface wind speed has been observed from multiple satellite instruments, including passive microwave radiometers and the active scatterometers (Zhang et al. 2006). The Department of Defense Meteorology Satellite Program (DMSP) passive microwave observations are from the onboard Special Sensor Microwave Imager (SSM/I; Hollinger et al. 1987; Wentz 1997). Later additions to these passive microwave observations include the Tropical Rainfall Measuring Mission (TRMM) Microwave Imager (TMI; Kummerow et al. 1998) and the Advanced Microwave Scanning Radiometer of the National Aeronautics and Space Administration's (NASA) Advanced Microwave Scanning Radiometer for Earth Observing System (EOS) (AMSR-E; e.g., Wentz and Meissner 2000). The scatterometer (e.g., NSCAT or QuikSCAT), which is active by nature, uses a microwave radar and retrieves both the wind speed

TABLE 1. The OceanSITES station IDs and attributes.

Station ID	WMO ID	Lat	Lon	Program	Records (daily)
08S067E	14040	-8.0°	67.0°	RAMA	284
00N080E	23001	0.0°	80.5°	RAMA	293
15N090E	23009	15.0°	90.0°	RAMA	363
32N145E	28401	32.4°	144.6°	KEO	306
00N165E	52321	0.0°	165.0°	TAO	357
00N170W	51010	0.0°	-170.0°	TAO	361
00N140W	51311	0.0°	-140.0°	TAO	364
15N038W	13008	15.0°	-38.0°	PIRATA	281
12N023W	13001	12.0°	-23.0°	PIRATA	365
00N023W	31007	0.0°	-23.0°	PIRATA	333
10S010W	15001	-10.0°	-10.0°	PIRATA	363

and wind direction (e.g., Dunbar et al. 1991a,b; Liu et al. 1998).

The number of long-term U.S. sea surface wind speed observing satellites has increased from one in July 1987 to five or more in 2000, on board various satellite programs. The multiple-satellite observations made it possible to generate globally gridded products, including the high-resolution winds produced routinely as a research product at NCDC (Zhang et al. 2006). This product has gained increased use throughout the research community in climate and oceanography efforts, as well as for applied applications such as the World Coral-Reef Watch and marine transportation/ship routing services.

The 6-hourly gridded winds are generated on a global $0.25^\circ \times 0.25^\circ$ grid over ice-free oceans (65°S – 65°N) (blended winds hereafter). The swath wind speeds were retrieved by Remote Sensing Systems, Inc. (RSS). RSS has been processing climate-research-quality satellite ocean winds (at 10-m height above sea level) from various satellite instruments (e.g., SSM/Is, TMI, QuikSCAT, and AMSR-E), funded by NASA's Data Pathfinder and Making Earth System Data Records for Use in Research Environments (MEaSUREs) programs, etc. For our analysis year of 2009, data retrieved from satellite measurements made by the AMSR-E, SSM/I on board the DMSP *F-13* satellite, TMI, and QuikSCAT were downloaded from the RSS website (<ftp://ftp.remss.com>), and are used in constructing the 2009 blended wind speed fields. In this analysis, wind directions from NCEP–Department of Energy (DOE) Reanalysis II (NRA-R2) are used in the decomposition of the blended wind speed in the east–west and south–north wind components. The blended winds are the 10-m equivalent neutral winds (Wentz 1997; Wentz and Meissner 2000; Zhang et al. 2006). The satellite retrievals are physically based, and no buoy data are used. However, a small correction has been applied to the SSM/I wind speeds to match the buoy winds on a yearly basis (Wentz et al. 2007).

c. NWP winds from international operational centers

The NWP winds are short-range forecast 10-m surface winds (NWP winds hereafter) from three participating operational NWP centers: ECMWF, the German Weather Service (Deutscher Wetterdienst, DWD), and the Japan Meteorological Agency (JMA).

The ECMWF data are obtained from the operational global atmospheric model, which is a hydrostatic spectral model based on the ECMWF Integrated Forecasting System. In 2009, it had a spectral resolution of T799, roughly equivalent to a gridpoint spacing of 25 km with 91 levels in the vertical from about 10 m to 0.01 hPa

(Untch et al. 2006). The latest operational resolution since January 2010 is T1279 (16 km). The initial conditions for the forecasts are obtained from the advanced four-dimensional variational data assimilation system (Bauer et al. 2010). The quality of the ECMWF tropical winds has recently been assessed (Bechtold et al. 2012).

The DWD's global numerical weather prediction model (GME) is a hydrostatic gridpoint model operating on an icosahedral–hexagonal grid. Hence, the mesh size is almost uniform across the whole globe (Majewski et al. 2002). In 2009 the mesh size was 40 km and the model had 40 levels from 10 m to 10 hPa. (In the current operational version, however, the resolution is 20 km with 60 levels to 5 hPa.) The dry parts of GME's equations are solved by semi-implicit Euler integration whereas semi-Lagrangian advection is employed for the humidity variables (Majewski et al. 2002).

The NWP wind data from JMA are an operational forecast product of its Global Spectral Model (GSM; Nakagawa 2009). GSM is JMA's operational NWP model for short- and medium-range forecasts covering the entire globe, and its resolution is TL959L60, approximately 20 km in the horizontal with 60 layers up to 0.1 hPa in the vertical. GSM runs 4 times a day, and provides 216-h (9-day) forecasts at 1200 UTC and 84-h forecasts at 0000, 0600, and 1800 UTC. A four-dimensional variational data assimilation (4DVAR) system is employed to provide initial fields to GSM (Iwamura and Kitagawa 2008).

For this SURFA project, all NWP winds have been interpolated by the NWP centers onto the same global $0.25^\circ \times 0.25^\circ$ grid as the blended winds, prior to their data submission into the SURFA data repository, making it easier for end users to intercompare those products. All forecast runs used in this study started at 1200 UTC. Thus, the forecast winds at 12, 15, 18, 21, 24, 27, 30, and 33 h correspond to winds at 0000, 0300, 0600, 0900, 1200, 1500, 1800, and 2100 UTC of the following day. The daily winds are obtained by averaging those 3-hourly winds. As the NWP models assimilate the OS winds in some way when producing their analyses (i.e., initial conditions) for forecasts, NWP winds are not completely independent of the OS winds.

d. Winds from the NCEP Climate Forecast System Reanalysis

The surface winds from the latest reanalysis produced by NCEP, referred to as CFSR, are also included in the comparison (CFSR winds hereafter). A number of improvements from its predecessors are associated with this reanalysis product, including a 6-hourly coupling between the atmosphere and ocean, an interactive sea ice model, and higher spatial and temporal model outputs

(Saha et al. 2010). The CFSR winds are 10-m winds on the T382 grid with a grid spacing of about $0.31^\circ \times 0.31^\circ$ in the tropics. The CFSR winds are interpolated bilinearly onto the OceanSITES locations. The daily winds are averaged from 0000, 0300, 0600, 0900, 1200, 1500, 1800, and 2100 UTC winds to be consistent with the temporal resolution of NWP winds. The OS winds from all but station 32N145E are generally assimilated into the CFSR winds and therefore the CFSR winds are not independent of the OS winds.

3. Buoy winds adjustment

The OS winds are measured at a height of 4 m, while the blended satellite, NWP, and CFSR winds are 10-m winds. There are a number of methods for adjusting the buoy winds in height. The methods can range from a simple approach assuming a logarithmically varying wind profile as a function of the roughness length (Peixoto and Oort 1992) to a more sophisticated approach that also takes atmospheric stability into consideration (Liu and Tang 1996; Fairall et al. 2003).

The simple logarithmical height-adjustment methods are primarily based on Monin–Obukhov similarity theory, which assumes that the surface fluxes in the surface layer are uniform with height. The wind speed at a height z is given by

$$U_z = [\ln(z/z_o)/\ln(z_{\text{ref}}/z_o)]U_{\text{ref}},$$

where U_z is the wind speed at height z , z_o is the momentum roughness length, and U_{ref} is the observed wind speed at height z_{ref} .

In reality, the surface fluxes are rarely uniform in the surface layer. They are affected by the atmospheric stability, which can be influenced by the surface sea state, as well as air–sea temperature and moisture contrasts. The more general wind speed dependence on height is therefore normally expressed as

$$U_z = U_s + (u_*^*/k)[\ln(z/z_o) + \varphi(z, z_o, L)],$$

where U_s is the surface speed (e.g., the surface current over ocean); u_*^* is the surface friction velocity, which is the square root of the kinematic stress; k is the von Kármán constant that has a value of 0.4; and φ is an atmospheric stability term, which is a function of the momentum roughness length, z_o , and the Monin–Obukhov scale length L .

Mears et al. (2001) demonstrated that the mean difference between the wind speeds corrected with the sophisticated method and corrected with the simple logarithmical method is about 0.12 m s^{-1} , with a standard

deviation of 0.17 m s^{-1} . This bias is shown to be largely independent of the buoy wind speed. Kara et al. (2008) have compared the performance of three commonly used sophisticated algorithms: Coupled Ocean–Atmosphere Response Experiment, version 3.0 (COARE3.0), Bourassa–Vincent–Wood (BVW), and Liu–Katsaros–Businger (LKB) within the context of air–sea stability effects over the global ocean. [A good review of the current state of the algorithms and detailed descriptions of these three algorithms can be found in Brunke et al. (2003).] The performance from these three algorithms was found to be quite similar globally; the local difference can be large, especially in the regions near the Kuroshio and Gulf Stream current systems (Kara et al. 2008).

The satellite-based winds are 10-m equivalent neutral-stability winds relative to the surface currents while the NWP and reanalysis winds are estimates of the actual winds at 10 m. The surface currents may have a positive/negative impact linearly to actual winds depending on their relative directions to the winds. The NWP 10-m winds have been shown to be about 0.2 m s^{-1} lower than the satellite-based 10-m winds (Mears et al. 2001; Chelton and Freilich 2005) while the localized impact of surface current to the 10-m adjusted buoy winds could be as large as 0.5 m s^{-1} (Chelton et al. 2004; Kelly et al. 2001; Cornillon and Park 2001; Hersbach and Bidlot 2008). Hersbach and Bidlot (2008) have also pointed out that the impact of surface currents can be quite systematic in the tropics because the relative direction between the winds and currents is quite persistent, resulting in a positive bias in winds in the tropical Pacific Ocean but a negative bias in both the tropical Atlantic and Indian Oceans in ECMWF data, although the biases tend to be less than 0.5 m s^{-1} . As the majority of the OceanSITES buoys are located in the tropical regions away from the Kuroshio and Gulf Stream, the impact of height-adjusted 10-m winds due to different algorithms is expected to be less than 0.5 m s^{-1} . More quantitative analysis on the surface current's effect on the height-adjusted 10-m winds will be shown later in this section.

In this study, the COARE3.0 algorithm (Fairall et al. 2003) is used to adjust 4-m buoy wind speeds to 10-m neutral wind speeds, which are computed as

$$U_{10m} = [u_*^*/(G^{1/2}k)]\ln(10/z_o),$$

where G is the gustiness factor (Fairall et al. 2003).

Peng et al. (2011) used the simple logarithmical approach to adjust the buoy winds from 4 to 10 m based on Peixoto and Oort (1992) with a typical oceanic value of $1.52 \times 10^{-4} \text{ m}$ for the roughness length. This practice tends to overestimate the adjusted buoy wind speeds

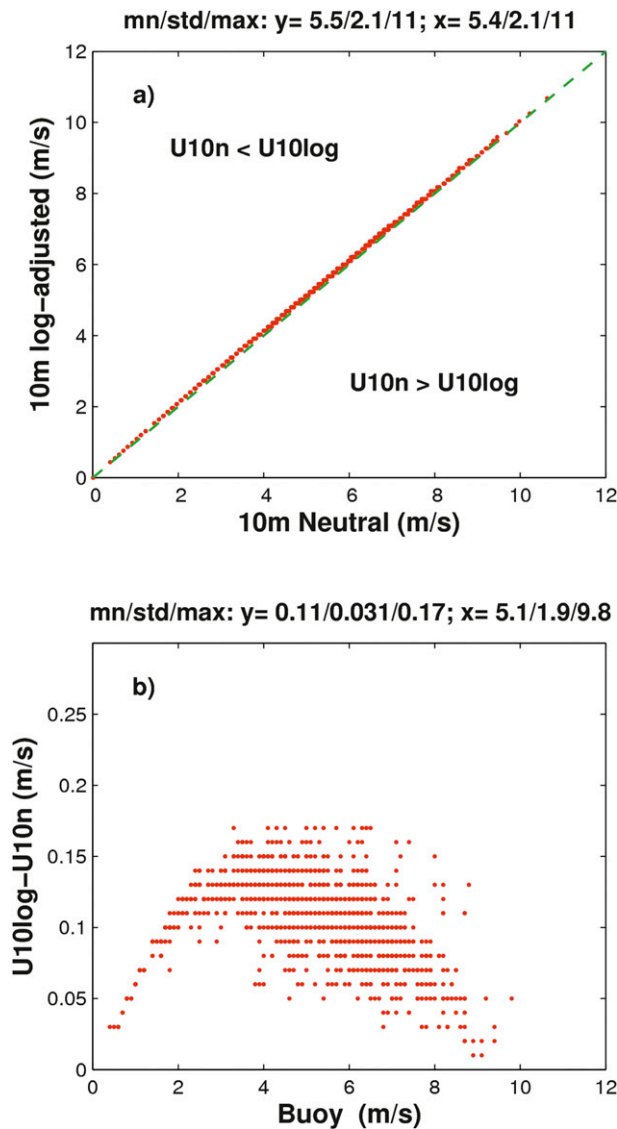


FIG. 2. (a) The scatter diagram for 2009 of 10-m buoy wind speeds adjusted logarithmically with a constant roughness length ($U10log$, vertical axis) and 10-m neutral buoy wind speeds adjusted using COARE3.0 ($U10n$, horizontal axis) for the three OceanSITES buoy stations in the equatorial Pacific Ocean used in Peng et al. (2011) and (b) distribution of the difference between the two adjusted 10-m wind speeds over 4-m observed buoy wind speeds.

slightly (Fig. 2). For these three locations in the equatorial Pacific Ocean, the difference between simple log-adjusted wind speeds and 10-m neutral wind speeds utilizing the COARE3.0 algorithm is less than 0.17 m s^{-1} , with a mean difference of about 0.11 m s^{-1} (Fig. 2b).

The time series of daily 4-m OS winds for all 11 locations are shown in Fig. 3a. As expected, the mid-latitude winds (station 32N145E) are dominated by

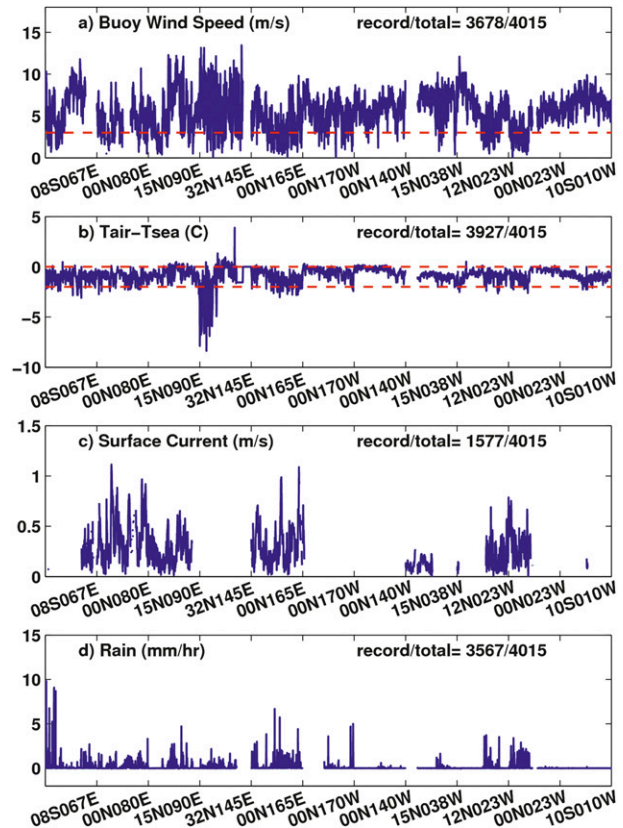


FIG. 3. The daily evolution of 2009 measurements at the buoy sites: (a) wind speeds (m s^{-1}), with dashed line denoting 3 m s^{-1} ; (b) near-surface air-sea temperature differences ($^\circ\text{C}$), with dashed lines denoting the 0° to -2°C range; (c) surface current speeds (m s^{-1}); and (d) rain rate (mm h^{-1}). In the plot, the numbers for the “record/total” are in days, which indicate the valid record count over the total possible record count.

more variability from synoptic scales as compared to the less-variable tropical winds. The majority of the air-sea temperature differences are within 0° to -2°C , except at station 32N145E, where the difference can be as large as -8°C (Fig. 3b). Thus, according to Kara et al. (2008), the impact of the air-sea temperature difference on the 10-m adjusted neutral winds from 4-m buoy winds is expected to be within 0.5 m s^{-1} and the difference between the 10-m adjusted neutral winds and 10-m actual winds is less than 0.3 m s^{-1} .

Among the 11 OceanSITES stations used in this analysis, there are 4 with little or no surface current data available, 4 with less than 50% surface current measurements available, and only 2 with good surface current temporal coverage for 2009 (more than 85% of data available) (Fig. 3c). As illustrated by May and Bourassa (2011), surface currents into the winds tend to enhance the resultant 10-m neutral winds and vice versa. The direct linear dependency of adjusted winds on surface

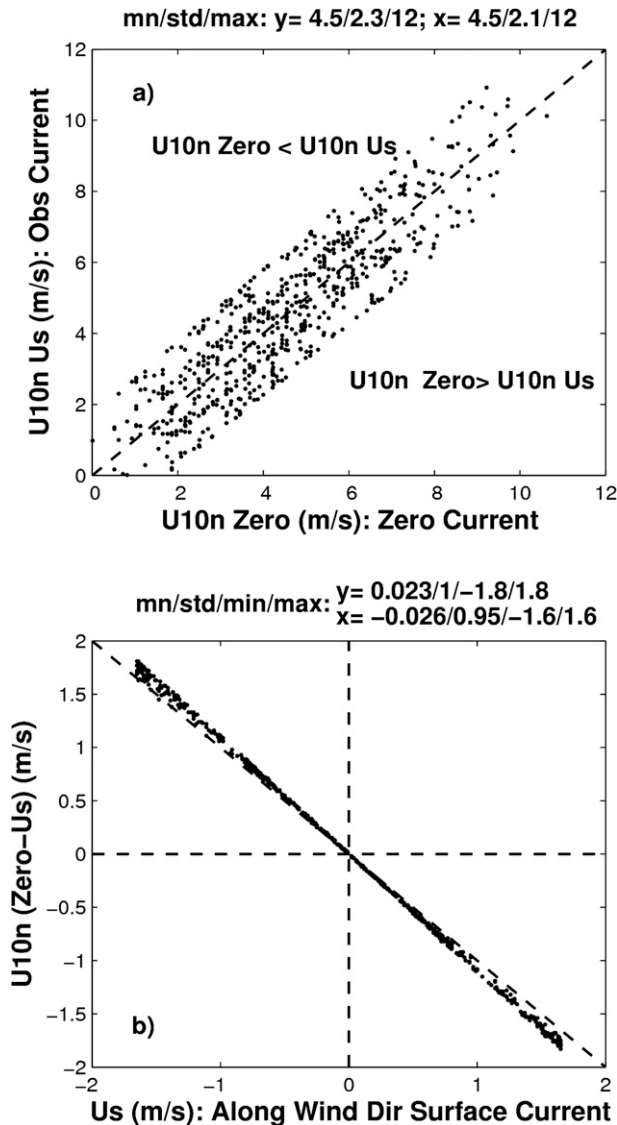


FIG. 4. (top) Scatter diagram of 10-m neutral buoy winds with and without observed surface currents and (bottom) the difference between the two as a function of the along-wind direction surface current speeds for the 00N080E and 00N165E stations during 2009.

currents is evident in Fig. 4, using the COARE3.0 package for the two stations that have good coverage of surface current data for 2009 (stations 00N080E and 00N165E). The averaged difference between 10-m neutral winds with or without observed surface currents is merely 0.02 m s^{-1} with a standard deviation of about 1 m s^{-1} for these two tropical stations (Fig. 4).

Station 32N145E, however, deserves special attention due to its proximity to the Kuroshio. As shown in Fig. 3c, no surface current data are available for 2009 at this site; however, the 15-m-depth subsurface current data existed about 80% of the time for 2009, and we use this

dataset as a proxy to examine the potential current effect on the winds. The 15-m current data are plotted in Fig. 5 (top panels) together with the monthly means derived from the Global Drifter Program (http://www.aoml.noaa.gov/phod/dac/dac_meanvel.php). Figure 5, including the power spectral density plots shown in the bottom panels, reveals that the monthly climatology based on the drifter data does not capture the synoptic-scale variability. A scatter diagram of adjusted 10-m neutral wind speeds using 15-m subsurface currents (U10n-Us) versus the ones with zero surface currents (U10n-Zero) is shown in Fig. 6. It shows that there is no distinct systematic bias between the two. The 2009 mean bias of 10-m adjusted neutral wind speeds with and without currents is minimal ($\sim 0.02 \text{ m s}^{-1}$), even at this location.

Due to the insufficient availability of surface current data for most of the buoys for 2009 and the minimal and similar impact on the mean bias that is expected for all NWP and reanalysis wind products, surface currents are set to be zero in this analysis. We will treat wind speed biases of 0.5 m s^{-1} or smaller as within the uncertainty level associated with unresolved processes, measurement accuracy, or parameterizations.

The time series of COARE3.0-adjusted 10-m neutral buoy winds are shown in Fig. 7a. The 10-m neutral wind speeds, on average, are about 0.4 m s^{-1} higher than the 4-m buoy wind speeds (Fig. 7b). The differences between the full COARE3.0 adjusted 10-m neutral winds and the simple logarithmically adjusted winds are within 0.2 m s^{-1} , except at station 32N145E where a small portion of the difference values exceed 0.2 m s^{-1} , associated with a higher than 2°C positive air-sea temperature difference (Fig. 7c).

4. Results

The evaluation of various wind products is carried out using commonly employed statistical metrics defined by World Meteorological Organization (WMO) for weather and climate model evaluations (WMO 1999; Phillips et al. 2004). These metrics include the mean, bias, standard deviation, root-mean-square (RMS) errors, and cross-correlation coefficients, using the OS winds as our reference time series.

a. Global spatial distribution of means and standard deviations

Before we show the statistical analysis results with point measurements, it is beneficial to provide large-scale patterns for the five products considered in this paper and differences among them. The 2009 mean and standard deviation of the zonal and meridional CFSR winds are displayed in the top panels in Figs. 8a and 8b,

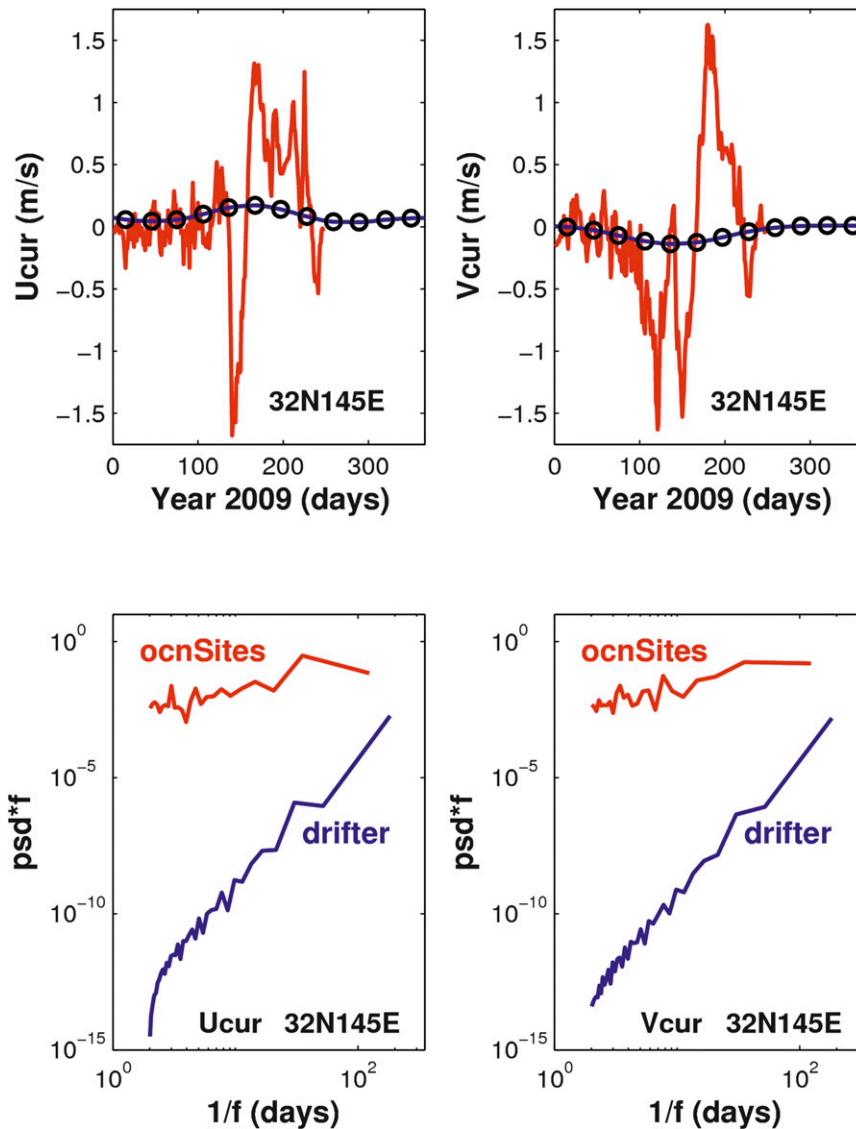


FIG. 5. (top) Time series and (bottom) power spectral density of near-surface (left) zonal and (right) meridional currents (red solid lines) at 32N145E during 2009. The circles are monthly climatological values of surface currents derived from drifters (data source: http://www.aoml.noaa.gov/phod/dac/dac_meanvel.php). The blue solid lines are for curve-fitted daily surface currents.

respectively. Global distributions of both 2009 means and their standard deviations are remarkably similar for all five wind products with largely westward mean equatorial winds. Therefore, distributions of differences between the CFSR winds and the other four products are shown in the bottom four panels of Figs. 8a and 8b, instead. The high mean bias tends to be located near landmasses, more so in the polar regions (both Arctic and Antarctic). The standard deviations are relatively small in the tropical regions as expected. The noticeable difference in standard deviation occurs, again, near landmasses, more so in

the polar regions as well, particularly for the blended winds (Figs. 8a and 8b, bottom panels). This is likely to be associated with some artifacts of satellite measurements or retrieving algorithms in dealing with ice. The 11 stations examined in this paper are located within extratropics and in the open ocean away from the coastal regions, thus avoiding the potential near-land-region artifacts. Overall and when referenced to the CFSR winds, the model-based products are close to each other and tend to underestimate the temporal variability, while the blended satellite winds exhibit high variability.

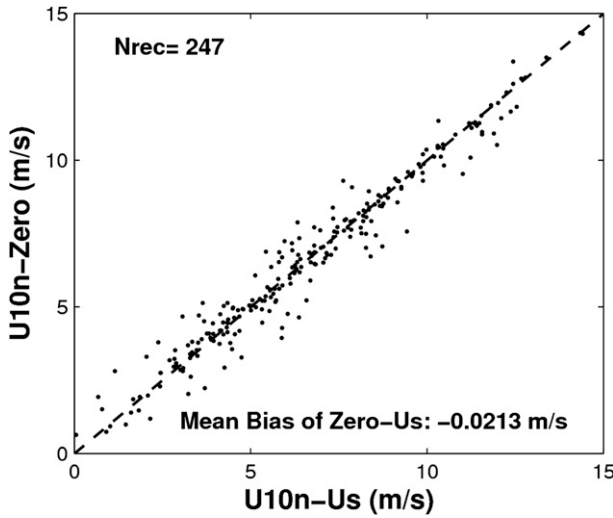


FIG. 6. Scatter diagram of adjusted 10-m neutral buoy wind speeds using 15-m near-surface currents ($U_{10n}-U_s$) versus the ones with zero surface currents ($U_{10n}-Zero$) at 32N145E during 2009.

b. Annual means and biases

The time series of daily OS wind components are displayed in Fig. 9. As expected, the midlatitude winds are dominated by the more dynamic synoptic variability as compared to the less-variable tropical winds. The seasonal cycles are more pronounced in the tropical Indian and Atlantic Oceans than are those in the tropical Pacific Ocean. There are relatively long data gaps in the time series of several stations, such as at 8°S, 67°E (13 October–31 December), 15°N, 38°W (1 January–25 March), and 32.4°N, 144.6°E (3 November–31 December), that may potentially lead to an alias in computing annual means at these stations.

In this paper, the biases are defined in terms of the means of the residuals (i.e., the differences between winds from each product and the OS 10-m neutral buoy winds). The margin of error associated with unresolved processes is about 0.5 m s^{-1} and results presented below should be interpreted within this context, and the focus will be on biases that are larger than 0.5 m s^{-1} and significant at the 95% confidence level.

As shown in Fig. 10a, the 2009 mean zonal winds are quite similar for all wind products at each equatorial station except for station 00N165E, where JMA and ECMWF show overly strong easterly winds. The biases from the OS zonal winds are mostly less than 0.5 m s^{-1} (Fig. 10b). The most notable exceptions are the ECMWF and JMA winds at station 00N165E with biases of about -1.1 m s^{-1} , which are significant at the 95% confidence level. The JMA winds at 12N23W also show a large bias of -0.95 m s^{-1} . Others with biases larger

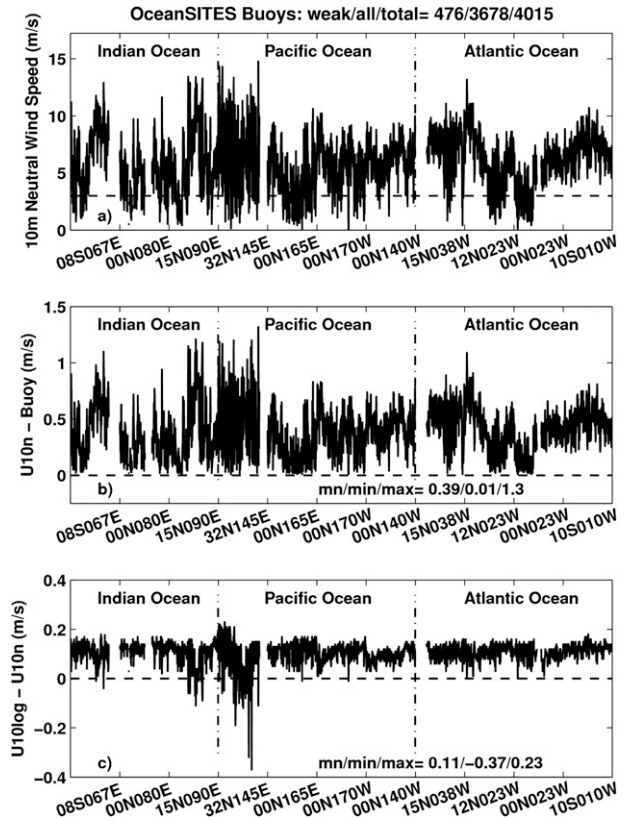


FIG. 7. The time series of (a) COARE3.0-adjusted 10-m neutral buoy wind speeds (U_{10n}) during 2009, (b) difference between U_{10n} and 4-m buoy wind speeds, and (c) difference between simple log-adjusted with a constant roughness length (U_{10log}) and U_{10n} .

than 0.5 m s^{-1} include the CFSR winds at 140° and 23°W along the equator (biases of 0.65 and -0.63 m s^{-1} , respectively), blended satellite winds at 15N090E, and all but DWD zonal winds at 32N145E (all positive); this is significant because the mean OS winds are near zero at this location. All the bias values higher than 0.5 m s^{-1} are significant at the 95% confidence level. It is worth noting that bias values at the 00N023W and 10S010W locations are significant at the 95% confidence level, even if most of those values are less than 0.5 m s^{-1} (Fig. 10b). The magnitude of the averaged zonal wind bias over all selected buoy locations for each product is quite small, ranging from about 0.05 to 0.2 m s^{-1} with a mean of -0.03 m s^{-1} for all products at all locations (Table 2). Our results show that one should not be misled by small globally averaged mean biases; there are strong regional dependences, as shown also in Kara et al. (2008) and Hersbach and Bidlot (2008), and large biases that could occur even with small globally averaged biases. This result is not unique to the sea winds but is also revealed for satellite-retrieved sea surface temperatures (Zhang et al. 2004).

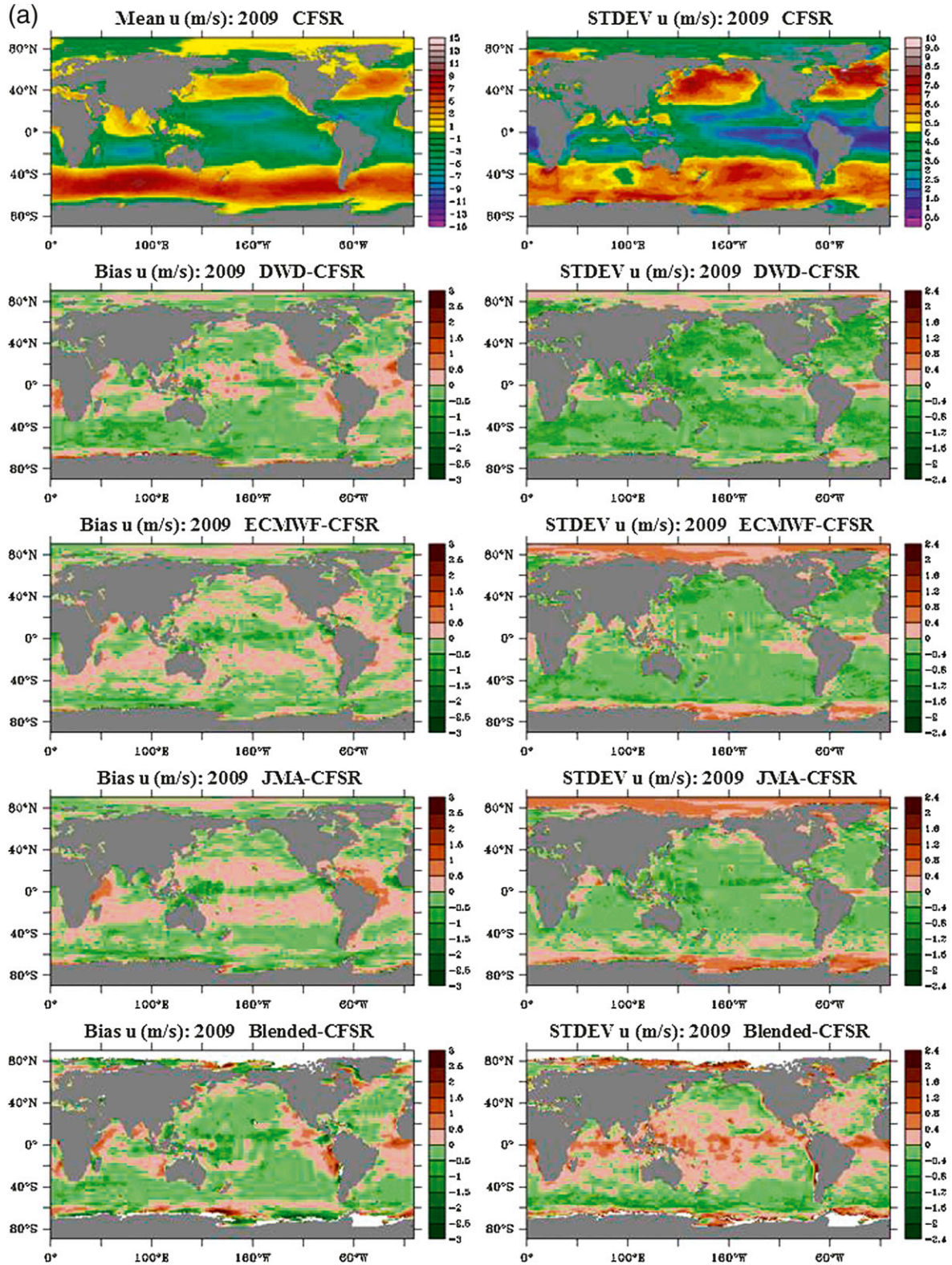


FIG. 8. (a) (top) Global spatial distribution of the mean and standard deviation of the 2009 CFSR zonal winds and the difference between the mean and standard deviation of the CFSR winds and that of the (top middle) DWD, (middle) ECMWF, (bottom middle) JMA, and (bottom) blended winds. (b) As in (a), but for the 2009 meridional winds.

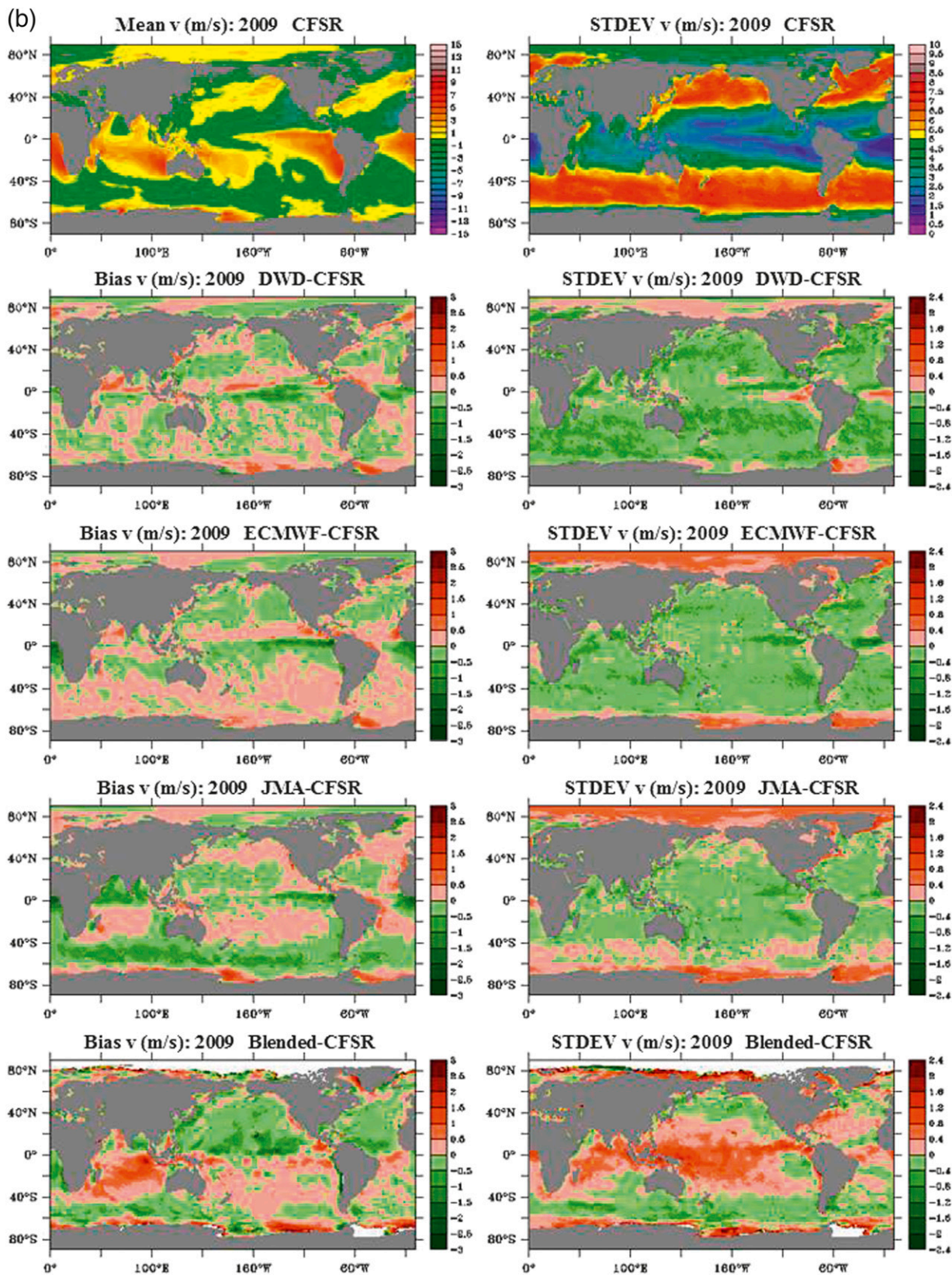


FIG. 8. (Continued)

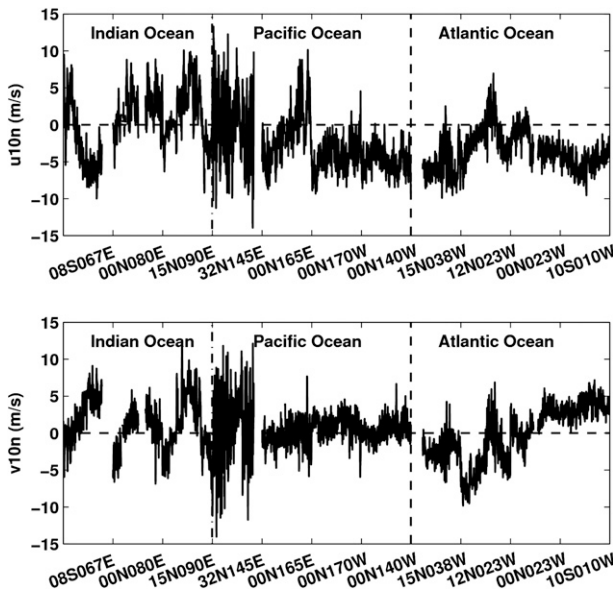


FIG. 9. Time series of COARE3.0-adjusted 10-m neutral buoy winds during 2009 in all 11 OceanSITES stations for the (top) zonal and (bottom) meridional components.

As shown in Fig. 11, the largest biases for the meridional winds are found at 00N170W (western Pacific warm pool region), which are larger than 0.5 m s^{-1} in magnitude for all wind products and have a mean of

-1.2 m s^{-1} ; all products failed to produce the nearly 2 m s^{-1} northward wind component. At the next station east, however, all products showed an overly northward wind component than that measured by the buoy at 00N140W, with a mean bias of 0.69 m s^{-1} . The bias values at both locations are significant at the 95% confidence level. At $12^\circ\text{N}, 23^\circ\text{W}$ in the Atlantic Ocean, the ECMWF and JMA winds failed to produce the strong southward wind component measured by the buoy, with mean biases larger than 0.5 m s^{-1} and statistically significant at the 95% confidence level. At 08S067E in the Indian Ocean, the DWD winds have the largest bias, just over 0.5 m s^{-1} but significant at the 95% confidence level. Also in the Indian Ocean at 00N080E, the JMA winds fall short of weak northward buoy winds while others overestimate the winds, resulting in the bias for JMA having the opposite sign compared to the others. Biases for both JMA and DWD, however, are significant at the 95% confidence level.

Once again, the magnitude of the averaged meridional wind bias for all locations for each product is small, ranging from about 0.006 to 0.055 m s^{-1} , with a mean of -0.03 m s^{-1} (Table 2), while large biases existed at about half of the 11 buoy locations.

c. Standard deviation and RMS errors

The standard deviation here is the square root of the variance of the time series of the wind component for

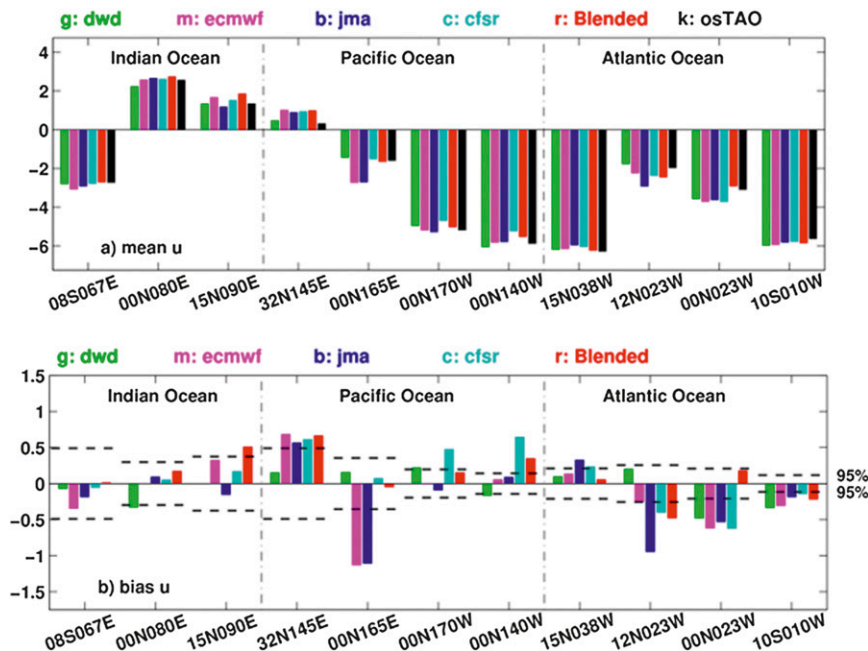


FIG. 10. Bar graph for the 2009 zonal winds: (a) means (m s^{-1}) and (b) biases (m s^{-1}). The plot is grouped by stations with different colors denoting different products: DWD (green), ECMWF (magenta), JMA (blue), CFSR (cyan), blended (red), and OS (black) winds. Bias values outside of the dashed lines for each station are significant at the 95% confidence level.

TABLE 2. The mean bias and cross-correlation coefficient values for each wind product.

	Blended	CFSR	ECMWF	DWD	JMA	All
u bias (m s^{-1})	0.12	0.09	-0.15	-0.048	-0.22	-0.03
v bias (m s^{-1})	-0.055	0.006	-0.05	-0.045	-0.035	-0.03
Speed bias (m s^{-1})	0.22	-0.14	-0.15	-0.24	-0.12	-0.07
Directional bias ($^{\circ}$)	-1.65	-0.25	-0.61	-1.15	0.87	-0.46
u cross correlation	0.89	0.95	0.92	0.87	0.90	0.91
v cross correlation	0.78	0.93	0.85	0.76	0.84	0.83

a specific product or observation. It measures the temporal variation magnitude from its own time mean for each wind product in our case. The standard deviation ratio (that of each product over the OS winds) is shown in Fig. 12; the standard deviation of the OS winds is printed in the plot for each station. As expected, the extratropical station at 32N145E has the highest standard deviation for the OS winds stations for both wind components, indicating large temporal variation associated with synoptic-scale weather systems compared to that of tropical stations. Even for those stations along the equator, the standard deviation ratios are within the same range as those for other stations, indicating that the model and satellite products captured the high wind variability relatively well over the tropical and midlatitude stations.

One of the general features in Fig. 12 is that, the blended satellite product (red) and the model-based product (NWP and reanalysis) are often on opposite sides of the OS wind variability (dashed line of ratio = 1): the former has a variability close to or higher than that of

the OS winds (i.e., the standard deviation ratio values are close to or higher than 1), while the model-based winds mostly show lower variability than that of the OS winds. This is particularly clear in the meridional winds (Fig. 12b). Note that the OS measured time series is normally continuous within 1 day; thus, the daily averaged winds may be closer to the true daily mean. In comparison, satellite observations are normally more discrete over time with spatial gaps between swaths; more studies are needed to diagnose the reasons for the higher blended satellite wind variability and whether it is caused by inadequate observation (subsampling aliases), or potential data spikes, as have been revealed in the past in other regions. In the next version of the blended satellite winds, more quality controls will be implemented to remove data noise. On the other hand, while the blended satellite winds correspond to a roughly 25-km wind, NWP forecast winds cannot resolve well spatial scales of less than four grid cells (i.e., 100 km). In addition to the numerical smoothing in NWP models, the models tend

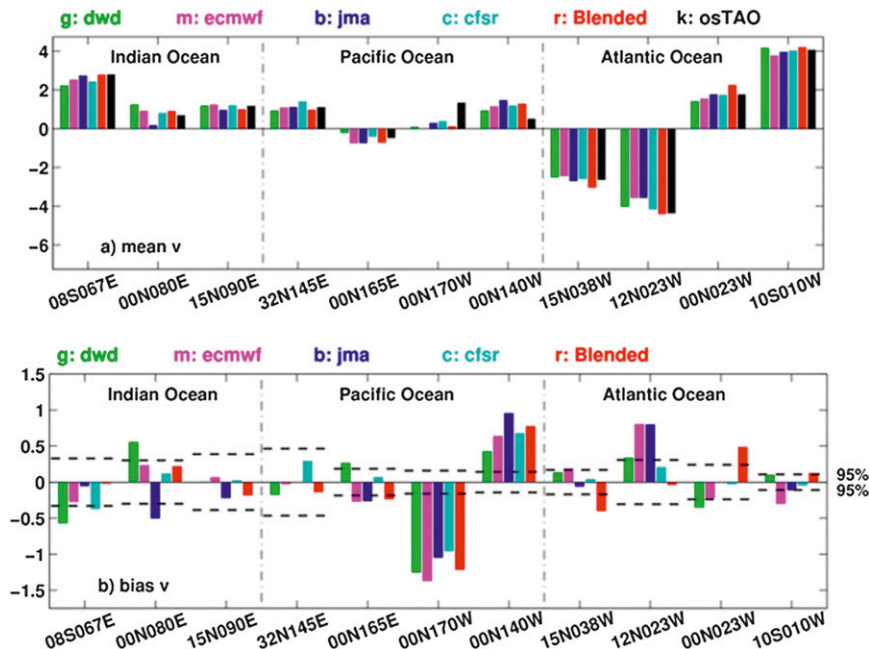


FIG. 11. As in Fig. 10, but for the 2009 meridional winds.

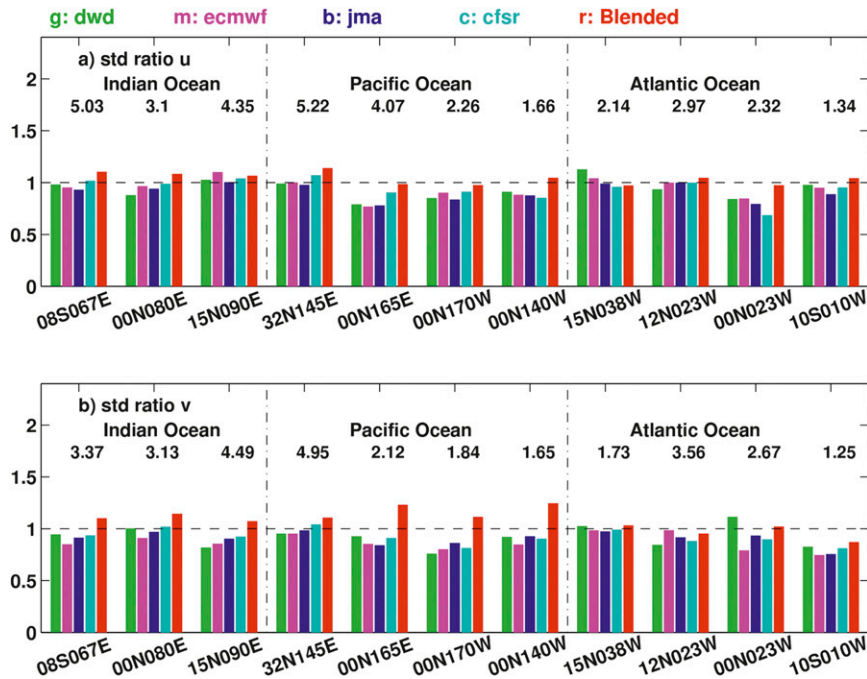


FIG. 12. Bar graph of the standard deviation ratio of the wind product over a buoy during 2009: (a) zonal and (b) meridional winds. The mean values of the buoy standard deviation are printed above the bars for each station.

to undersimulate the spatial variability, which has been known to the modeling communities based on the past literature. This shortcoming still prevails across the board and is an area to be improved upon.

The RMS error is defined as the square root of the variance of the residuals from the OS time series. The RMS error measures the extent to which the wind values differ from the buoy measurements statistically. RMS

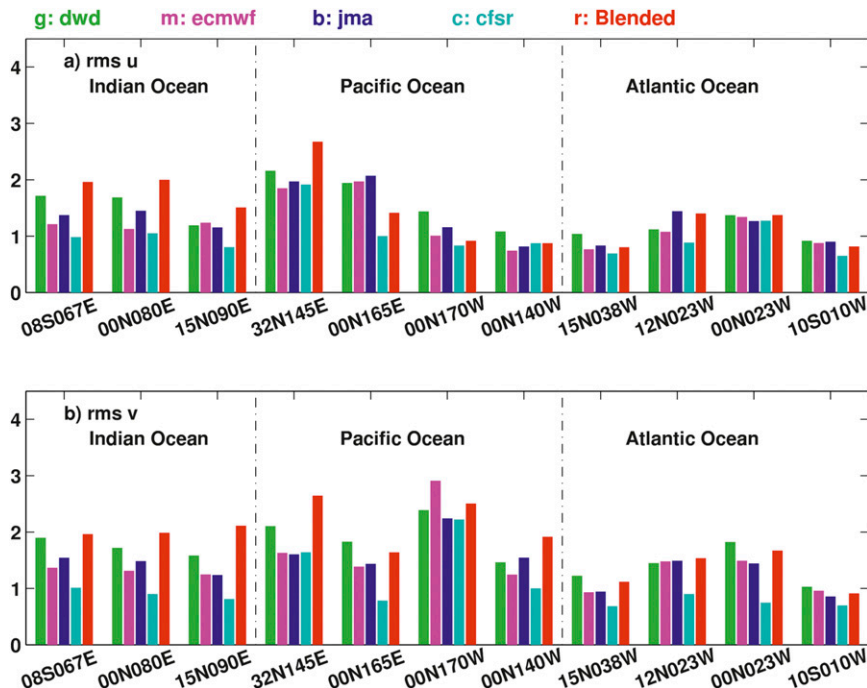


FIG. 13. Bar graph of RMS errors of wind products from the buoys during 2009: (a) zonal and (b) meridional winds.

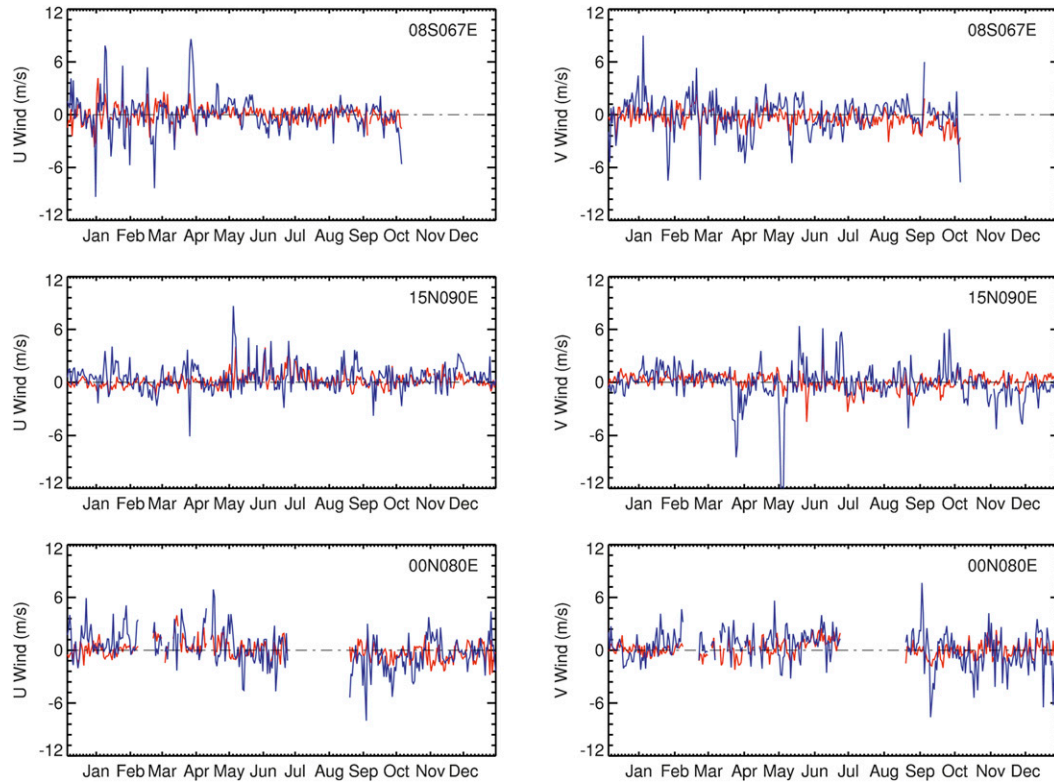


FIG. 14. Time series of 2009 wind residual from the OS winds for the CFSR winds (red) and the blended winds (blue) for the three locations in the Indian Ocean. Shown are (left) zonal and (right) meridional winds.

errors have been widely used in the evaluation of data products as a measure of accuracy. As shown in Fig. 13, the RMS errors for the CFSR winds are overall smaller than for other wind products. The RMS errors for the blended winds tend to be larger than others in the tropical Indian Ocean for both zonal and meridional winds, while the results are mixed for the other two basins.

Figure 14 shows the time series of wind residuals for the CFSR (red) and blended (blue) winds. While the time series of the wind residual for the CFSR winds are mostly confined within a -2 to 2 m s^{-1} range, they are quite noisy for the blended winds, with large spikes that are larger than 5 m s^{-1} in magnitude. The difference could be, in part because the CFSR winds are restrained by buoy winds via a data assimilation scheme, while the blended winds are not. Rain has been known to be one of the significant factors that degrade satellite-based wind retrievals, especially for scatterometer data as the radar backscattering measurements are augmented by additional backscatter from both atmospheric rain and surface rain perturbations (Weissman et al. 2002; Draper and Long 2004). There is some indication that the scattering by rain could be one of the influence factors for generating those spikes. However, it does not

appear to be the dominant factor from our analysis, as shown in Fig. 15. Closer examination revealed that some of those large spikes are caused by the wind direction errors when decomposing the blended wind speeds into $u-v$ components using the NRA-2 wind directions. (When the blended satellite product was developed, CFSR was not available and NRA-2 has been updated operationally at NCEP and is thus used.) Figure 16 displays the scatter diagrams of blended (left panels) and CFSR (right panels) winds with the OS winds for all three stations in the Indian Ocean. The records falling in the II and IV quadrants denote the days when the blended or CFSR winds are at least 90° from those of the OS buoys. A striking feature is that outliers in those two quadrants are associated with large residuals (greater than 3 m s^{-1} , denoted by a crisscross; Fig. 16). While the occurrence for the CFSR winds is very minimal (2 and 1 out of 940 valid records, less than 0.2%), it ranges from 3.3% to 4.3% for the blended satellite speed-NRA-2 wind directions. Note that NRA-2 has coarse grid spacing ($\sim 2^\circ$), which poorly resolves the spatial variability associated with synoptic- and small-scale systems (Chelton et al. 2004; Peng 2004; Dukhovskoy and Bourassa 2011). (Results for the ECMWF winds are

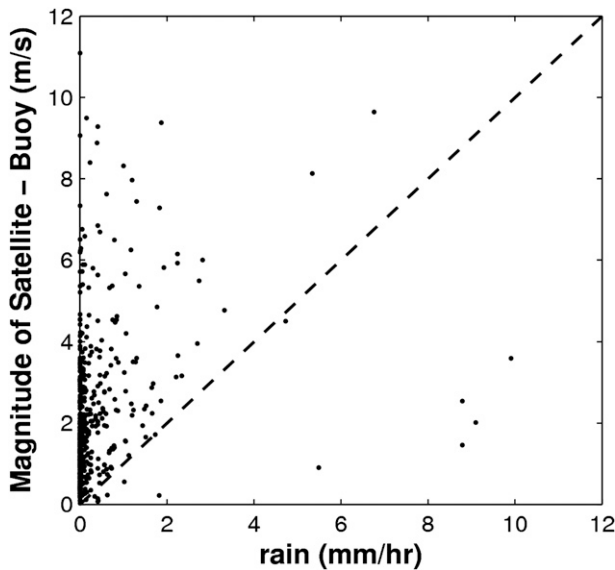


FIG. 15. The scatter diagram of the magnitude of the 2009 blended wind residual from the OS winds for the three locations in the Indian Ocean as a function of rain rate.

similar to that of the CFSR winds and thus are not shown.) For future improvements to the blended wind product, a weather and single-pixel filtering method taking rain flags into consideration could be used to reduce those large spikes, together with using directions from a high-resolution reanalysis such as CFSR for historical reprocessing, and high-resolution operational analysis such as the NCEP Climate Forecast System (CFS) or the ECMWF model for near-real-time processing or monitoring (as currently used for the near-real-time version), to minimize the impact of the directional error effects. In addition, a new and improved version of the satellite-retrieved wind speeds has just been released by RSS (www.remss.com); an updated version of the blended product is planned using the new satellite retrievals.

d. Cross-correlation coefficients

Cross correlation is a standard method of estimating the degree to which two series covary with each other. Our analysis shows that the maximum cross-correlation coefficients between all wind products and the OS winds occur at the zero lag (not shown), implying no systematic phase shift in the wind products. The cross-correlation coefficients between the CFSR winds and OS winds are the highest, ranging from 0.88 to 0.99 for the zonal winds and 0.83 to 0.99 for the meridional winds (Fig. 17). Overall, the correlations are high (above ~ 0.76) for all the products for the zonal winds, as well as for the meridional winds for most stations other than the three

tropical Pacific stations and one South Atlantic station, where correlations are slightly lower. The wind patterns are dominated by zonal winds in those regions and the variations are well captured by the model and satellite products. On the other hand, the meridional winds are weaker, and the variations are slightly less well captured by the wind products other than the CFSR, which may have assimilated the buoy observations well. All values of the cross-correlation coefficients are statistically significant at the 95% confidence level.

In contrast to the tropical Pacific stations, large wind synoptic variability observed in the midlatitude KEO station in both the zonal and meridional directions is well captured by all the wind products studied here (correlation of above 0.88). With generally high temporal variation associated with synoptic variability, as displayed in the standard deviation (Fig. 12), this may imply that all wind products are able to capture well the synoptic temporal variability in their winds—a very encouraging aspect.

e. Bias of wind speed and direction

Figure 18 shows the means of wind speeds, and the means of the speed and wind direction residuals (difference between speeds or wind directions of a wind product and the OS winds). The weak winds (wind speed $< 3 \text{ m s}^{-1}$) are not included in the calculations of the directional bias due to the large uncertainty associated with the resultant wind direction. For the wind speed, the satellite-based blended product generally overestimates the speeds compared to the OS observed values, while the model-based products generally underestimate the speeds (Figs. 18a and 18b). The average speed bias for the blended winds is about 0.23 m s^{-1} higher than that of the OS winds while the other four winds are $0.12\text{--}0.24$ lower with a spread of about 0.4 m s^{-1} (Table 2), which is consistent with the previous study. The spread of the speed bias for individual stations can be larger than 1 m s^{-1} (Fig. 18b). [Chelton and Freilich \(2005\)](#) showed that 10-m wind speeds from the ECMWF analysis are systematically lower than those of satellite (NSCAT) observations for the periods of August 1999–July 2000 and February 2002–January 2003. Our results here have indicated that the same is true for the ECMWF short-range forecast winds, along with the JMA and DWD short-range forecast winds, as well as the CFSR reanalysis winds for the period of January–December 2009. Based on [Chelton and Freilich \(2005\)](#), a wind speed bias of 0.4 m s^{-1} could increase the wind stress bias by more than 10%, which could potentially induce erroneous ocean currents and states from ocean models driven by these model products.

Keeping with meteorological convention, wind directions are expressed in degrees clockwise from north,

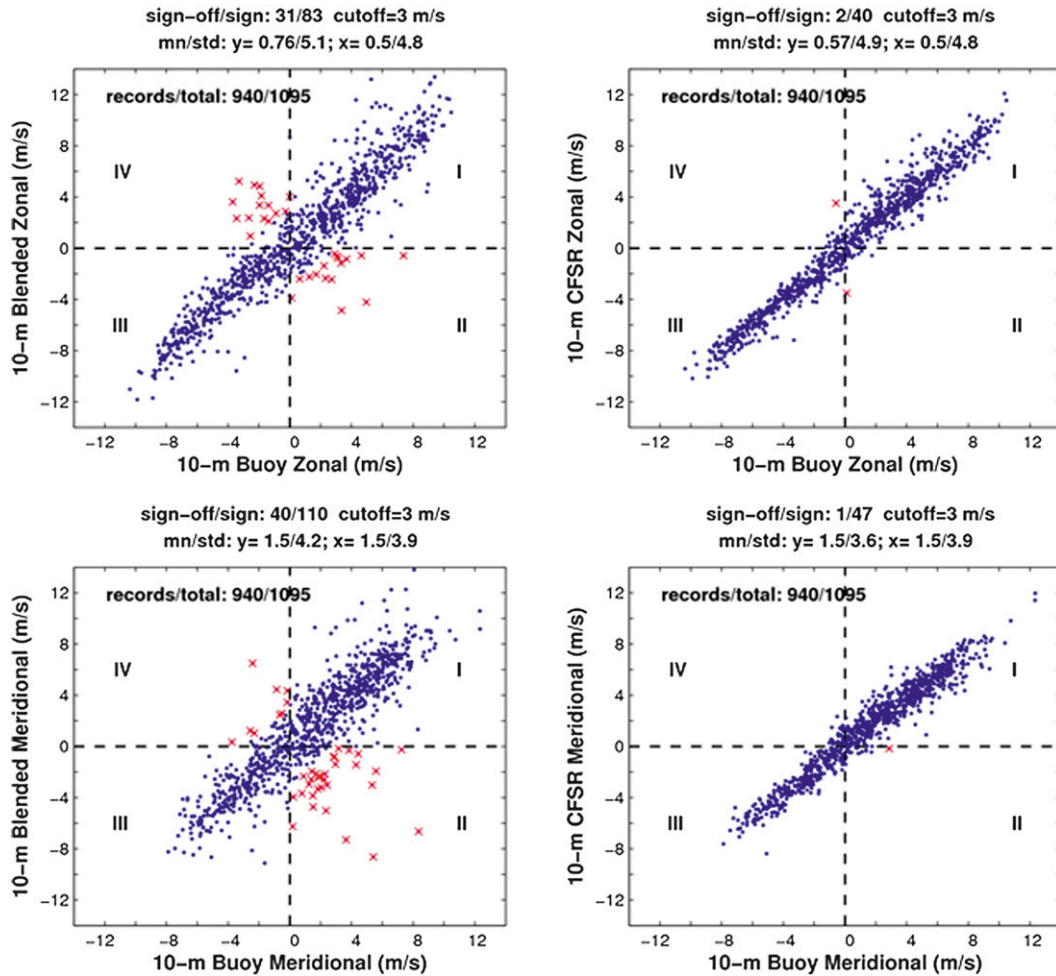


FIG. 16. The scatter diagrams of 2009 (left) blended winds and (right) CFSR winds with 10-m buoy winds for the three locations in the Indian Ocean. The (top) zonal and (bottom) meridional winds. The crisscross marks the record when the blended or CFSR wind directions are at least 90° away from that of the buoy winds and with wind speed residuals higher than 3 m s⁻¹.

describing the direction from which the wind is blowing. For example, a wind with $u = -2 \text{ m s}^{-1}$ and $v = -2 \text{ m s}^{-1}$ would be expressed as 45°.

Directional anomalies A_n are calculated relative to buoy winds by

$$A_n = D_n - D_b,$$

where D_n represents the direction given by each wind product and D_b represents the direction given by the buoy. Thus, $A_n = -10^\circ$ corresponds to a situation in which the direction given by a wind product is 10° counterclockwise to that of the buoy. Anomaly values are adjusted such that $-180^\circ < A_n \leq 180^\circ$, which is occasionally necessary when the values given by a wind product and the buoy are on opposite sides of north.

The wind direction biases are shown in Fig. 18c, computed as the annual mean of the directional anomaly A_n for 2009. Figure 18c does not show any global systematic biases for any individual product; that is, the averaged biases can be both positive and negative. On the other hand, the biases tend to be station dependent. For example, in the extratropical Pacific Ocean, the 32N145E buoy station reveals negative directional biases for all products with the bias value of -9.62° for the blended winds being significant at the 95% confidence level, the 12N023W buoy station in the tropical Atlantic Ocean reveals positive directional biases for all products with the bias value of 9.67° for the JMA winds being significant at the 95% confidence level, and in the tropical Indian Ocean the 08S067E station reveals negative directional biases for all products but the blended

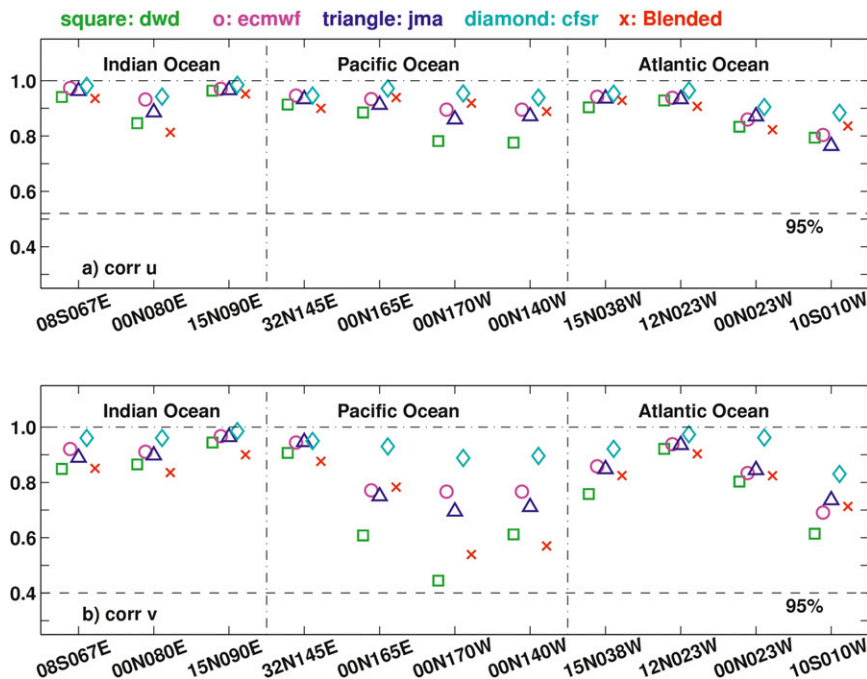


FIG. 17. The cross-correlation coefficients for (a) zonal and (b) meridional winds between each wind product and OS winds during 2009.

winds and the 15N090E buoy station reveals positive directional biases for all products except the blended winds (all bias values are not statistically significant at the 95% confidence level). The largest directional bias occurs at 0° , 170°W with the means of the wind direction residuals being in a range from -9.94° for CFSR to -13.89° for ECMWF with an average value of -10.09° for all products (Table 3). A positive bias is observed at 0° , 140°W with the means of the wind direction residuals in a range of 3.25° for DWD to 8.8° for JMA, with an average value of 5.31° for all products. With mean wind directions of about 105° and 95° for the osTAO winds at 0° , 170°W and 0° , 140°W , respectively, a negative bias of -10° will reduce the meridional winds at 0° , 170°W and a positive bias of 5.31° will increase the meridional winds at 0° , 140°W , which contributes to the negative (positive) values we have seen in the biases of the meridional winds at 0° , 170°W (0° , 140°W). The more critical implication will be that it may potentially induce an artificial local stress curl and, therefore, could generate spurious upper-ocean circulation if used to drive ocean models, which was first noted by Peng et al. (2011).

Figure 19 shows a complementary cumulative distribution function, illustrating how often each wind product deviates from the buoy direction by at least a given amount (in degrees). For example, the CFSR winds (shown in light blue) deviate from buoy-observed winds by at least

20° in 5.6% of cases, while the blended winds (i.e., NRA-2 directions, shown in red) deviate by the same amount in 21.2% of the cases. It clearly shows the improvement of the latest NCEP reanalysis over its predecessor.

The speed and directional biases shown in Fig. 18 are computed using scalar averaging where the wind speed and direction are treated separately as scalar values. As the wind is a vector quantity, another commonly used averaging is done by summing the u and v components that are derived from the wind speed and direction and averaging at the end of the averaging time (i.e., vector averaging).

During periods of moderate to high wind speeds, the difference between the vector and scalar averages will be small. In the case of wind speed, vector-averaged speeds will never be larger than the scalar-averaged values and will generally be lower. Larger differences could occur with greater wind direction variance, which typically occurs at lower wind speeds (below 2 m s^{-1}) (Gilhousen 1987). Figure 20 shows that the vector-averaged directional bias exhibits a larger variation than that of the scalar-averaged one, although the results from both methods tend to be consistent overall.

5. Summary and discussion

A data repository for collocated model forecasts, a satellite-based product, and in situ observations has

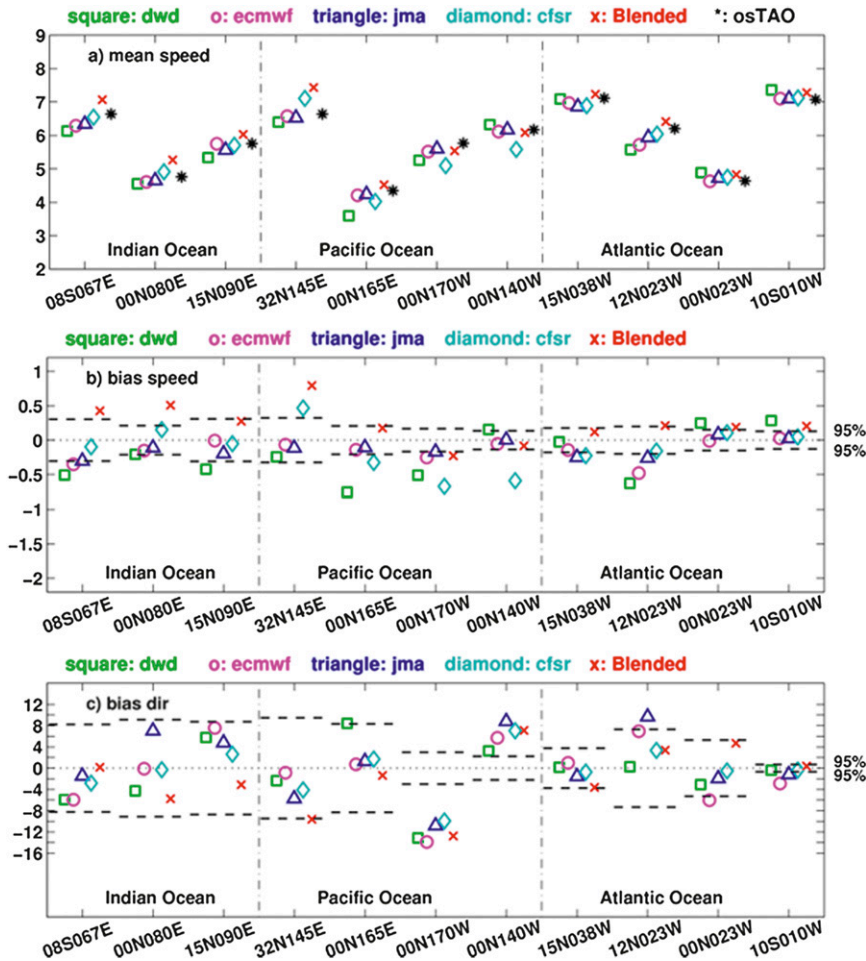


FIG. 18. (a) Speed mean, (b) speed, and (c) directional bias of 2009 surface winds. The weak winds (wind speed <math> < 3 \text{ m s}^{-1}</math>) are not included in the calculations of directional bias. Bias values outside of the dashed lines for each station are significant at the 95% confidence level.

been created at NCDC under the support of various WCRP working groups to facilitate the evaluation and monitoring of weather and climate model forecast skills and satellite-based products against high-quality in situ observations. Daily 2009 surface winds from five wind

products are compared with the measurements from 11 OceanSITES buoys located in the open oceans of the Indian, Pacific, and Atlantic basins. The primary objectives in this study are to provide some statistical measures of how well each of these wind products (or taken as

TABLE 3. The means of the wind direction residuals. The boldface italic values are significant at the 95% confidence level.

Station ID	DWD	ECMWF	JMA	CFSR	Blended	All products
08S067E	-5.91	-5.95	-1.47	-2.82	0.16	-2.66
00N080E	-4.27	-0.12	7.03	-0.29	-5.75	-0.57
15N090E	5.77	7.56	4.79	2.63	-3.13	2.94
32N145E	-2.35	-0.87	-5.71	-4.11	-9.62	-3.77
00N165E	8.44	0.72	1.30	1.70	-1.38	1.80
00N170W	-13.13	-13.89	-10.80	-9.94	-12.76	-10.09
00N140W	3.25	5.69	8.80	7.03	7.10	5.31
15N038W	0.16	0.98	-1.55	-0.73	-3.62	-0.79
12N023W	0.25	6.94	9.67	3.33	3.39	3.93
00N023W	-3.09	-6.04	-1.95	-0.53	4.70	-1.15
10S010W	-0.40	-2.88	-1.19	-0.37	0.39	-0.74

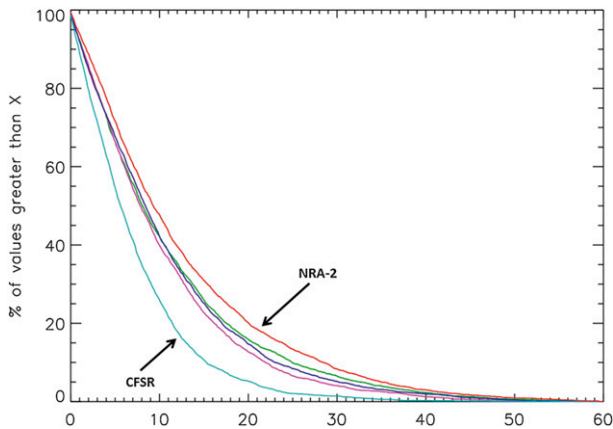


FIG. 19. Cumulative distribution function over the absolute directional anomaly ($^{\circ}$). The weak winds (wind speed $< 3 \text{ m s}^{-1}$) are not included in the calculations of directional bias: green is for DWD, magenta for ECMWF, blue for JMA, cyan for CFSR, and red for the blended winds.

a whole) performs against the high-quality reference in situ wind measurements and to uncover if any systematic bias in the wind products exists.

Our results have shown that the cross correlations between various wind products and the buoy winds are all above the 95% significance level, ranging from 0.76 to 0.99 for the zonal winds and 0.45 to 0.99 for the meridional winds. The correlation coefficients are high (at or above 0.76) for all products at the dynamic midlatitude, along the prevailing wind direction (zonal wind) at all of the buoy stations studied, as well as along the weak meridional directions at all but the three equatorial Pacific stations and the one Atlantic/PIRATA station in the south (10°S , 10°W). The cross correlations between the CFSR winds and the buoy winds are consistently higher than the others, with the overall smallest RMS errors, for both zonal and meridional winds. In contrast, the cross-correlation coefficients between the blended or DWD winds and the buoy winds are mostly lower than the others, especially so for the meridional winds (Table 2, Fig. 17). On the other hand, the blended wind product tends to have positive mean wind speed biases compared to all the model results (Fig. 18b).

This analysis reveals the strong and weak aspects of the blended product (and the model results as well) and, thus, directions for future improvements. Work has begun at NCDC to improve the blended satellite-based winds according to the results shown in this study. For some oceanography and meteorology studies and applications, gradients and derivative of surface winds, such as wind stress and its associated curl, are also critically important. Intercomparison of these parameters derived from the different products discussed here is desirable and could serve as a future research topic.

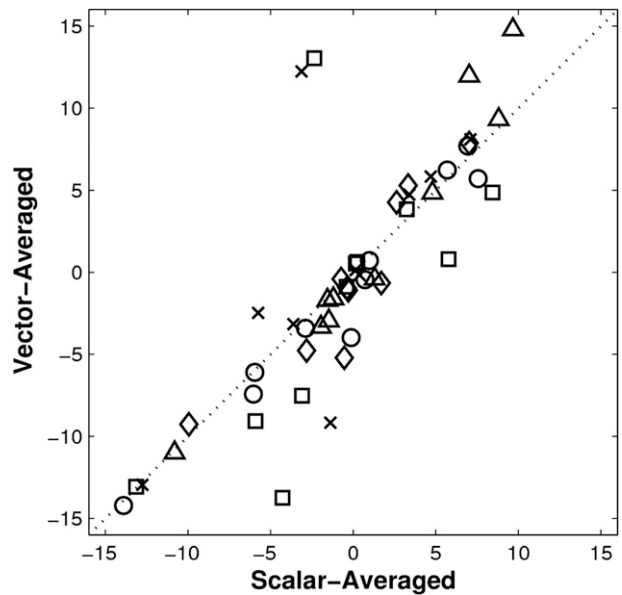


FIG. 20. Scatter diagram of 2009 directional bias computed from vector and scalar averaging: DWD (squares); ECMWF (circles); JMA (triangles); CFSR (diamonds); and blended (crosses).

All of the model-based wind products constrain their winds (and/or other variables) by either buoy and/or satellite data to a certain degree. The CFSR and ECMWF models assimilate both remotely sensed data as well as in situ measurements, although the assimilation schemes and datasets used may differ. The DWD model assimilates buoy winds with satellite scatterometer winds assimilated since July 2009. The JMA model only assimilates satellite scatterometer data for 2009. The NWP winds are short-range forecast winds from analyses that are constrained by the observations. The blended winds are based on the remotely sensed wind speed with wind directions taken from NRA-2, which also assimilates both remotely sensed and in situ data. This may contribute to the fact that the overall characteristics of all wind products examined here are fairly similar and the correlations are high.

It is very encouraging that the magnitude of the wind component bias for all wind products is now less than 1.4 m s^{-1} and the majority of those are within 0.5 m s^{-1} , which is a significant improvement compared to 3.1 m s^{-1} , thanks to improvements in the models, observations, and data assimilation capability. The magnitude of the wind component biases averaged over all the stations is less than 0.03 m s^{-1} . All five wind products examined here compare well with each other and correlate well with the OS winds, especially for the zonal winds, with the CFSR winds being closely fitted to the OS winds. This, again, may be in part due to the similarity among the sources from which these wind products are based on or derived. The performance of the three NWP

forecasts is quite comparable, particularly so between the ECMWF and JMA winds.

However, our analysis has also revealed that all the meridional winds have systematic negative (positive) biases at 0°, 170°W (0°, 140°W). These biases are associated with the consistent negative/positive biases in wind directions at these locations and are significant at the 95% confidence level. These directional biases do not appear to be related to the known alignment error associated with the instruments for the TAO buoy winds that was described in Freitag et al. (2001). Brown et al. (2005) have indicated that systematic directional errors could be a result in ECMWF short-range forecasts, as wind turning across the marine atmospheric boundary layer is systematically underestimated. There are also negative directional biases at 32.4°N, 144.6°E and positive directional biases at 12°N, 23°W. The directional biases of opposite signs are observed at 8°S, 67°E and 15°N, 90°E, which would potentially induce a spurious regional wind stress curl. However, the majority of those biases are not significant at the 95% confidence level.

Even though the 11 OceanSITES stations are spread across the Indian, Pacific, and Atlantic Ocean basins, caution should be taken when applying the conclusions in this paper globally. In addition, because the wind speeds are mostly less than 13.8 m s^{-1} , the results should not be extended to high-wind conditions.

As shown in this study, the average magnitude of biases for each wind product for all stations could be very small (less than 0.03 m s^{-1} for both the zonal and meridional winds), while the values for each individual station could be as high as 1.2 m s^{-1} for the zonal winds and 1.4 m s^{-1} for the meridional winds. This implies that only looking at a collective value, as many studies in the literature do, could have provided us with a more optimal picture than the analysis of individual stations could reveal. While it is necessary to carry out this analysis on a large quantity of stations or to examine the global characteristics of the selected variables, it is also crucial to examine a number of carefully selected stations in more detail to get a more representative picture, as we have done in this study. The caveat is that near-uniform statistical characteristics do not necessarily imply uniform characteristics and performance in resolving individual weather events, especially in fast-evolving and fast-moving events such as tropical convection associated with westerly wind bursts. In fact, they can be very different in terms of determining the correct timing and location for an individual NWP forecast product (J.-R. Bidlot 2012, personal communication).

Acknowledgments. The analysis was carried out at NOAA's NCDC, supported in part by the NCDC Climate

Data Record Program through the Cooperative Institute for Climate and Satellites—North Carolina under Cooperative Agreement NA09NES4400006. We thank ECMWF, DWD, and JMA for providing their model datasets and the NCDC NOMADS team for the NCEP/CFSR data. We thank Chris Fairall for providing us with the COARE 3.0 package and help in implementing the package and Diane Stokes for the information on the use of buoy data in the NCEP/CFSR winds. The blended winds can be obtained online (<http://www.ncdc.noaa.gov/oa/rsad/air-sea/seawinds.html>). The OceanSITES and the NWP model datasets can be downloaded online (<ftp://eclipse.ncdc.noaa.gov/pub/surfa/>). We thank Dr. Meghan Cronin for identifying the metadata error at the KEO (32N145E) station and for providing us with the correct station metadata.

We thank Richard Reynolds, Detlev Majewski, and Ken Knapp for beneficial discussions and comments. The comments and suggestions from the NCDC internal reviewers have enhanced the clarity of this paper. The constructive suggestions from Dr. Meghan Cronin and two other anonymous WAF reviewers and the editor have resulted in greatly enhanced analysis and improved clarity of the paper. Ferret, a product of NOAA's Pacific Marine Environmental Laboratory, was used for analysis.

REFERENCES

- Abdalla, S., P. A. E. M. Janssen, and J.-R. Bidlot, 2011: Altimeter near real time wind and wave products: Random error estimation. *Mar. Geod.*, **34**, 393–406.
- Bauer, P., A. J. Geer, P. Lopez, and D. Salmond, 2010: Direct 4D-Var assimilation of all-sky radiances. Part I: Implementation. *Quart. J. Roy. Meteor. Soc.*, **136**, 1868–1885.
- Bechtold, P., and Coauthors, 2012: Progress in predicting tropical systems: The role of convection. ECMWF Tech. Memo. 685, ECMWF, Reading, United Kingdom, 61 pp.
- Bourassa, M. A., and Coauthors, 2010: Remotely sensed winds and wind stresses for marine forecasting and ocean modeling. *Proceedings of OceanObs'09: Sustained Ocean Observations and Information for Society Conference*, J. Hall, D. E. Harrison, and D. Stammer, Eds., Vol. 2, ESA Publ. WPP-306, doi:10.5270/OceanObs09.cwp.08.
- Bourlès, B., and Coauthors, 2008: The PIRATA program: History, accomplishments, and future directions. *Bull. Amer. Meteor. Soc.*, **89**, 1111–1125.
- Brown, A. R., A. C. M. Beljaars, H. Hersbach, A. Hollingsworth, M. Miller, and D. Vasiljevic, 2005: Wind turning across the marine atmospheric boundary layer. *Quart. J. Roy. Meteor. Soc.*, **131**, 1233–1250.
- Brunke, M. A., C. W. Fairall, X. Zeng, L. Eymard, C. Laurence, and J. A. Cury, 2003: Which bulk aerodynamic algorithms are least problematic in computing ocean surface turbulent fluxes? *J. Climate*, **16**, 619–635.
- Chelton, D. B., and M. H. Freilich, 2005: Scatterometer-based assessment of 10-m wind analyses from the operational ECMWF and NCEP numerical weather prediction models. *Mon. Wea. Rev.*, **133**, 409–429.

- , M. G. Schlax, M. H. Freilich, and R. F. Miliff, 2004: Satellite measurements reveal persistent small-scale features in ocean winds. *Science*, **303**, 978–983.
- Cornillon, P., and K. A. Park, 2001: Warm core ring velocities inferred from NSCAT. *Geophys. Res. Lett.*, **28**, 575–578.
- Cronin, M. F., C. Meinig, C. L. Sabine, H. Ichikawa, and H. Tomita, 2008: Surface mooring network in the Kuroshio Extension. *IEEE Syst. J.*, **2**, 424–430.
- Curry, J. A., and Coauthors, 2004: SEAFLUX. *Bull. Amer. Meteor. Soc.*, **85**, 409–424.
- Dickinson, S., K. A. Kelly, M. J. Caruso, and M. J. McPhaden, 2001: Comparison between the TAO buoy and NASA Scatterometer wind vectors. *J. Atmos. Oceanic Technol.*, **18**, 779–806.
- Donohue, K. A., and Coauthors, 2008: Program studies the Kuroshio Extension. *Eos, Trans. Amer. Geophys. Union*, **89**, 161–162.
- Draper, D. W., and D. G. Long, 2004: Evaluating the effect of rain on SeaWinds scatterometer measurements. *J. Geophys. Res.*, **109** (C12), doi:10.1029/2002JC001741.
- Dukhovskoy, D., and M. Bourassa, 2011: Comparison of ocean surface wind products in the perspective of ocean modeling of the Nordic Seas. *Proc. Oceans 2011*, Waikoloa, Hawaii, IEEE, 110430-002.
- Dunbar, R. S., S. V. Hsiao, and B. H. Lambrigtsen, 1991a: Science algorithm specifications for the NASA Scatterometer project: Sensor algorithms. JPL D-5610-1, Jet Propulsion Laboratory, Pasadena, CA, 694 pp.
- , —, and —, 1991b: Science algorithm specifications for the NASA Scatterometer project: Geophysical algorithms. JPL D-5610-2, Jet Propulsion Laboratory, Pasadena, CA, 388 pp.
- Ebuchi, N., H. C. Craber, and M. J. Caruso, 2002: Evaluation of wind vectors observed by QuikSCAT/SeaWinds using ocean buoy data. *J. Atmos. Oceanic Technol.*, **19**, 2049–2062.
- Fairall, C. W., J. E. Hare, A. A. Grachev, and J. B. Edson, 2003: Bulk parameterization of air–sea fluxes: Updates and verification for the COARE algorithm. *J. Climate*, **16**, 571–591.
- Freilich, M. H., and R. S. Dunbar, 1999: The accuracy of the NSCAT 1 vector winds: Comparisons with National Data Buoy Center buoys. *J. Geophys. Res.*, **104** (C5), 11 231–11 246.
- , and B. A. Vanhoff, 2006: The accuracy of preliminary WindSat vector wind measurements: Comparisons with NDBC buoys and QuikSCAT. *IEEE Trans. Geosci. Remote Sens.*, **40**, 622–637.
- Freitag, H. P., M. O’Haleck, G. C. Thomas, and M. J. McPhaden, 2001: Calibration procedures and instrumental accuracies for ATLAS wind measurements. NOAA Tech. Memo. OAR PMEL-119, 20 pp.
- Gilhousen, D. B., 1987: A field evaluation of NBDC moored buoy winds. *J. Atmos. Oceanic Technol.*, **4**, 94–104.
- Hersbach, H., and J.-R. Bidlot, 2008: The relevance of ocean surface current in the ECMWF analysis and forecast system. *Proc. Workshop on Atmosphere–Ocean Interactions*, Reading, United Kingdom, ECMWF, 61–73. [Available online at http://www.ecmwf.int/publications/library/ecpublications/_pdf/workshop/2008/Atmos_Ocean_Interaction/Hersbach.pdf.]
- Hollinger, J., R. Lo, G. Poe, R. Savage, and J. Pierce, 1987: Special Sensor Microwave/Imager’s user’s guide. NRL Tech. Rep., 120 pp.
- Iwamura, K., and H. Kitagawa, 2008: An upgrade of the JMA Operational Global NWP model. *CAS/JSC WGNE Research Activities in Atmospheric and Oceanic Modelling*, No. 38, WMO, 6.3–6.4. [Available online at http://www.wcrp-climate.org/WGNE/BlueBook/2008/chapters/BB_08_S6.pdf.]
- Josse, P., G. Caniaux, and S. Planton, 1999: Intercomparison of ocean–atmosphere fluxes from oceanic and atmospheric forced and coupled mesoscale simulations. *Ann. Geophys.*, **17**, 566–576.
- Kara, A. B., A. J. Wallcraft, and M. A. Bourassa, 2008: Air–sea stability effects on the 10 m winds over the global ocean: Evaluations of air–sea flux algorithms. *J. Geophys. Res.*, **113**, C04009, doi:10.1029/2007JC004324.
- Kelly, K. A., S. Dickinson, M. J. McPhaden, and G. C. Johnson, 2001: Ocean currents evident in satellite wind data. *Geophys. Res. Lett.*, **28**, 2469–2472.
- Kummerow, C., W. Barnes, T. Kozu, J. Shiue, and J. Simpson, 1998: The Tropical Rainfall Measuring Mission (TRMM) sensor package. *J. Atmos. Oceanic Technol.*, **15**, 809–817.
- Large, W. G., W. R. Holland, and J. C. Evans, 1991: Quasi-geostrophic response to real wind forcing: The effects of temporal smoothing. *J. Phys. Oceanogr.*, **21**, 998–1017.
- Liu, W. T., and W. Tang, 1996: Equivalent neutral wind. JPL Publ. 96-17, Jet Propulsion Laboratory, 16 pp.
- , —, and P. S. Polito, 1998: NASA Scatterometer provides global ocean–surface wind fields with more structures than numerical weather prediction. *Geophys. Res. Lett.*, **25**, 761–764.
- Majewski, D., D. Liermann, P. Prohl, B. Ritter, M. Buchhold, T. Hanisch, G. Paul, and W. Wergen, 2002: The operational global icosahedral–hexagonal gridpoint model GME: Description and high-resolution tests. *Mon. Wea. Rev.*, **130**, 319–338.
- May, J. C., and M. A. Bourassa, 2011: Quantifying variance due to temporal and spatial difference between ship and satellite winds. *J. Geophys. Res.*, **116**, C08013, doi:10.1029/2010JC006931.
- McPhaden, M. J., and Coauthors, 1998: The Tropical Ocean–Global Atmosphere (TOGA) observing system: A decade of progress. *J. Geophys. Res.*, **103** (C7), 14 169–14 240.
- , and Coauthors, 2009: RAMA: The Research Moored Array for African–Asian–Australian Monsoon Analysis and Prediction. *Bull. Amer. Meteor. Soc.*, **90**, 459–480.
- Mears, C. A., D. K. Smith, and F. Wentz, 2001: Comparison of Special Sensor Microwave Imager and buoy-measured wind speeds from 1987 to 1997. *J. Geophys. Res.*, **106** (C6), 11 719–11 729.
- Nakagawa, M., 2009: Outline of the high resolution global model at the Japan Meteorological Agency. RSMC Tokyo-Typhoon Center Tech. Review 11, 13 pp.
- Peixoto, J. P., and A. H. Oort, 1992: *Physics of Climate*. American Institute of Physics, 520 pp.
- Peng, G., 2004: Validation of a global reanalysis model in representing synoptic-scale eddies using scatterometer data: A case study. *Geophys. Res. Lett.*, **31**, L16201, doi:10.1029/2004GL020297.
- , C. N. K. Mooers, and H. C. Graber, 1999: Coastal winds in south Florida. *J. Appl. Meteor.*, **38**, 1740–1757.
- , H.-M. Zhang, H. P. Frank, J.-R. Bidlot, M. Higaki, and W. Hankins, 2011: A comparison of various equatorial Pacific surface wind products. *Proc. 2011 Int. Geoscience and Remote Sensing Symp.*, Vancouver, BC, Canada, IEEE, 2049–2052.
- Phillips, T. J., and Coauthors, 2004: Evaluating parameterizations in general circulation models: Climate simulation meets weather prediction. *Bull. Amer. Meteor. Soc.*, **85**, 1903–1915.
- Reynolds, R. W., K. Arpe, C. Gordon, S. P. Hayes, A. Leetmaa, and M. J. McPhaden, 1989: A comparison of tropical Pacific surface wind analyses. *J. Climate*, **2**, 105–111.
- Saha, S., and Coauthors, 2010: The NCEP Climate Forecast System Reanalysis. *Bull. Amer. Meteor. Soc.*, **91**, 1015–1057.
- Tang, W., W. T. Liu, and B. W. Stiles, 2004: Evaluation of high-resolution ocean surface vector winds measured by QuikSCAT

- scatterometer in coastal region. *IEEE Trans. Geosci. Remote Sens.*, **42**, 1762–1769.
- Untch, A., M. Miller, M. Hortal, R. Buizza, and P. Janssen, 2006: Towards a global meso-scale model: The high-resolution system T799L91 and T399L62 EPS. *ECMWF Newsletter*, No. 108, ECMWF, Reading, United Kingdom, 6–13.
- WCRP, 2012: Action plan for WCRP research activities on surface fluxes. WCRP Informal/Series Rep. 01/2012, 10 pp. [Available online at http://www.wmo.int/pages/prog/gcos/apocXVII/4a_Surface_Fluxes.pdf.]
- Weissman, D. E., M. A. Bourassa, and J. Tongue, 2002: Effects of rain rate and wind magnitude on SeaWinds scatterometer wind speed errors. *J. Atmos. Oceanic Technol.*, **19**, 738–746.
- Wentz, F. J., 1997: A well-calibrated ocean algorithm for SSM/I. *J. Geophys. Res.*, **102** (C4), 8703–8718.
- , and T. Meissner, 2000: AMSR ocean algorithm, version 2. RSS Tech. Rep. 121599A-1, Remote Sensing Systems, Santa Rosa, CA, 59 pp. [Available online at http://www.remss.com/papers/amr/AMSR_Ocean_Algorithm_Version_2.pdf.]
- , L. Ricciardulli, K. A. Hilburn, and C. A. Mears, 2007: How much more rain will global warming bring? *Science*, **317**, 233–235. [Supplementary material available online at <http://www.sciencemag.org/cgi/data/1140746/DC1/1>.]
- WMO, 1999: Commission for Basic Systems abridged final report with resolutions and recommendations. WMO Rep. 893, 184 pp. [Available online at www.wmo.int/pages/prog/www/ois/Operational_Information/Publications/CBS/CBS_Ext_893/893_en.pdf.]
- Zhang, H.-M., R. W. Reynolds, and T. M. Smith, 2004: Bias statistics of the AVHRR sea surface temperature. *Geophys. Res. Lett.*, **31**, L01307, doi:10.1029/2003GL018804.
- , J. J. Bates, and R. W. Reynolds, 2006: Assessment of composite global sampling: Sea surface wind speed. *Geophys. Res. Lett.*, **33**, L17714, doi:10.1029/2006GL027086.